AN ABSTRACT OF THE THESIS OF

Michele W. Winz for the degree of Doctor of Philosophy in Physics presented on August 27, 2003. Title: The Construction and Computational Modeling of a Fiber Bragg Grating Tunable Laser Diode.

Abstract approved: Redacted for privacy

Thomas K. Plant

The widespread adoption of wavelength division multiplexing to increase the bandwidth of optical fiber communication systems has provided a major impetus for research on low cost, single-mode, wavelength stable tunable diode lasers for use in optical telecommunications due to the large volume of lasers required. Other applications, such as demodulation of fiber Bragg grating sensor systems can also make use of inexpensive tunable laser diodes. In addition, the steady increase in the amount of computational power available has led to the widespread use of computers to model physical systems both to predict system performance and to gain insight into physical behavior.

Following a brief review of the application and construction of optical fiber Bragg gratings and a discussion of diode lasers and common methods of tuning diode laser wavelengths, a coupled-cavity approach to modeling laser diode output spectra, the construction of a fiber Bragg grating wavelength tunable laser, and the coupled cavity model of the fiber Bragg grating wavelength tunable diode laser are detailed. The physical laser system consists of a commercial Fabry-Perot diode laser with a cavity length of 300 microns, antireflection coated with a single layer of SiO, and coupled into an optical fiber containing a fiber Bragg grating. Wavelength tuning is accomplished by applying axial strain to the fiber grating. The coupled cavity model

directly includes the antireflection coating, includes the fiber Bragg grating as an index step, and is the first reported implementation of this method to model fiber Bragg grating coupled laser diodes. The measured output spectra of the physical laser diode system and the calculated output spectra are given and compared. Continuous tuning of the diode laser by applying axial strain to the fiber grating is not observed nor calculated to occur for a single-layer silicon monoxide antireflection coating. To achieve continuous wavelength tuning, better antireflection coatings will need to be developed.

The Construction and Computational Modeling of a Fiber Bragg Grating Tunable Laser Diode

by
Michele W. Winz

A THESIS

submitted to

Oregon State University

in partial fulfillment of
the requirements for the
degree of

Doctor of Philosophy

Presented August 27, 2003
Commencement June 2004

Doctor of Philosophy thesis of Michele W. Winz presented on August 27, 2003.

APPROVED:

Redacted for privacy

Major Professor, representing Physics

Redacted for privacy

Chair of the Department of Physics

Redacted for privacy

Dean of the Graduate School

I understand that my thesis will become part of the permanent collection of Oregon State University libraries. My signature below authorizes release of my thesis to any reader upon request.

Redacted for privacy

Michele W. Winz, Author

ACKNOWLEDGEMENTS

It is impossible for thesis research to be completed without substantial support and assistance from many sources. While it would be impossible to thank every person who has given me assistance, I would like a few people who have been instrumental in the completion of my thesis research. First and foremost, I would like to express sincere appreciation for Dr. Thomas K. Plant for serving as my Major Professor, providing me guidance throughout my research, assistance with my thesis, and taking our research group out to Sancho's for lunch. Without those big burritos, this thesis would never have been possible.

I would also like to thank Doug Ericksen and Kurt Stump, both members of our research group. Kurt Stump was the first graduate student working for Dr. Plant on the fiber Bragg gratings and is the one who brought me into all of this in the first place. He has since left OSU to work on a degree in Medical Physics. Doug Ericksen's hard work in the lab and unique view on life were invaluable in both the collection of data on the physical laser device as well as his willingness to have the computer program run on his computer, which yielded a substantial reduction in running time of the program. Doug is also the only individual that I have observed eat a "Big Gordo" burrito in one sitting.

My wife has been a constant support throughout my research and my thesis writing. She has reminded me when necessary that life consists of more than just research, while at the same time supporting and encouraging my efforts and convincing me to keep typing when I really wanted to take a little break for a month or two. My daughter, April, was also a help in this process, even though she is too young to understand how her happiness and little successes lifted me. Finally, I

would also like to thank my parents, Roger and LaDawna for encouraging me in my scholarly endeavors from a young age, reminding me that I had better go to college (or else!).

TABLE OF CONTENTS

TABLE OF CONTENTS (Continued)

LIST OF FIGURES

LIST OF FIGURES (Continued)

LIST OF FIGURES (Continued)

The Construction and Computational Modeling of a Fiber Bragg Grating Tunable Laser Diode

Chapter One

Introduction

Optical fiber Bragg gratings (FBGs) consist of a periodic perturbation to the index of refraction of the core of an optical fiber. This perturbation to the index of refraction along the core of the fiber allows an FBG to profoundly affect light traveling inside an optical fiber [1]. FBGs were discovered in 1978 when Hill *et al.* sent 488 nm light from an argon-ion laser into the core of a germanium-doped optical fiber [2]. Since the discovery of FBGs, much research has been conducted to examine the nature of the photosensitivity that allows grating construction, methods of writing FBGs, and applications of FBGs [3].

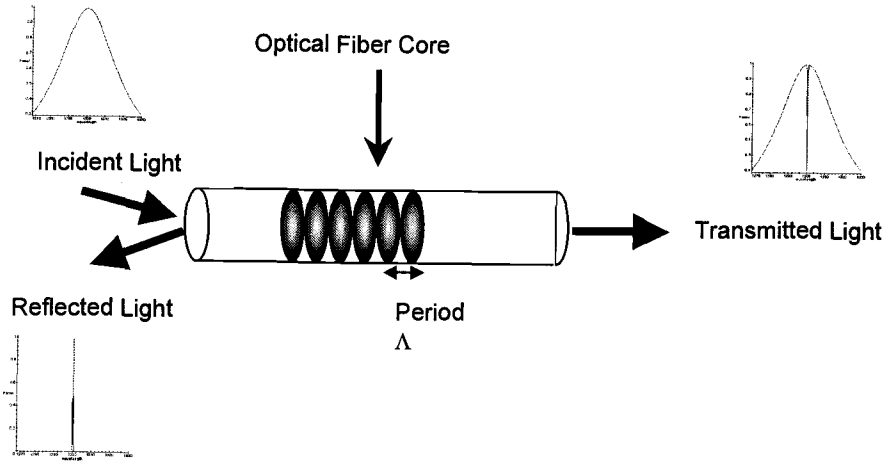

Figure 1.1 Diagram of optical fiber core illustrating periodic changes in index of refraction with period Λ as well as transmitted and reflected spectra for a typical optical fiber Bragg grating (After [4]).

The above figure illustrates the periodic index of refraction changes in an FBG along the length of the optical fiber, as well as typical transmission and reflection properties. For a broadband light source, the FBG reflects a narrow range of wavelengths back, at a wavelength given by the Bragg equation: $\lambda=2n_{eff}\Lambda$, with a corresponding dip in the transmitted signal. By changing either the periodicity of perturbations to the index of refraction (Λ), or the effective index of refraction (n_{eff}), the reflected wavelength (λ) can be changed. In addition to typical FBGs, tilted gratings, constructed by angling the changes in index of refraction causing light to be coupled into or out of the optical fiber, long period gratings that couple light into forward propagating optical fiber cladding modes, chirped gratings with broad spectral profiles and long lengths for both temporal pulse shaping and optical fiber sensor uses, and regular FBGs in unusual fibers such as polarization-maintaining fibers for sensor uses and rare earth doped fiber for pump, ASE (amplified spontaneous emission), and fiber laser sources, are available [3,4, and 6].

1.1 Optical fiber Bragg gratings in strain sensor systems

One application of FBGs is as sensing elements in optical fiber sensor systems. When used as the sensing element in an optical fiber sensor system, the dependence of the reflected wavelength on the periodicity of the index of refraction changes is employed. When an optical fiber with an FBG inscribed in the core is placed under tensile strain, the optical fiber elongates slightly, in proportion to the strain applied. This elongation of the fiber increases the period of the index of refraction changes in

the FBG and alters the index of refraction slightly due to strain-optic effects, thus changing the wavelength reflected by the FBG. The change in wavelength reflected by the FBG is measured and the applied strain calculated using Equation 1.1:

$$\Delta\lambda = \lambda(1 - p_e)\varepsilon_z, \tag{1.1}$$

where ε_z is the applied axial strain, λ is the wavelength reflected by the FBG, $\Delta\lambda$ is the change in wavelength reflected due to the applied strain, and p_e is the effective strain-optic coefficient[3]. Wavelength response is approximately 1.2 picometers per microstrain for gratings written at 1550nm.

Due to the large expense, complexity, and size of laboratory instruments capable of measuring the wavelength shift to picometer accuracy, a second FBG is often used in an FBG sensor system to "demodulate" the signal of the sensor FBG and translate the change in wavelength of the sensing grating to a change in optical power, which can be measured with a photodiode [7]. This demodulation method is illustrated in Figure 1.2, below.

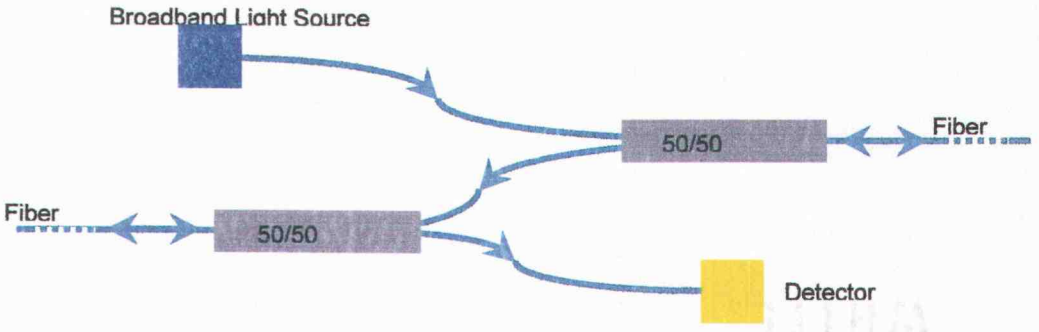

Figure 1.2 Schematic illustrating components in a simple FBG sensor demodulation system. One FBG is used as the sensing element, while the other grating is used as a reference. Arrows indicate direction of light propagation.

To illustrate how the two grating demodulation system codes wavelength change into an optical power change, Figures 1.3a-c plot the reflection spectra of two FBGs of slightly different wavelengths as well as the light that is reflected by both gratings. In the first plot, both gratings are close in center wavelength, and the amount of light that is reflected off of both gratings and thus makes it to the sensor is substantial, as shown by the yellow shaded area. The second and third plots illustrate the decreasing amount of power that makes it to the detector as the sensing (blue) grating is strained. As the sensing grating is strained to longer wavelengths, the yellow shaded area representing the power that reaches the detector decreases in size. Since the signal out of a reverse-biased photodiode optical detector is proportional to the amount of light incident upon the detector, the signal produced by the detector decreases as the sensing FBG is strained.

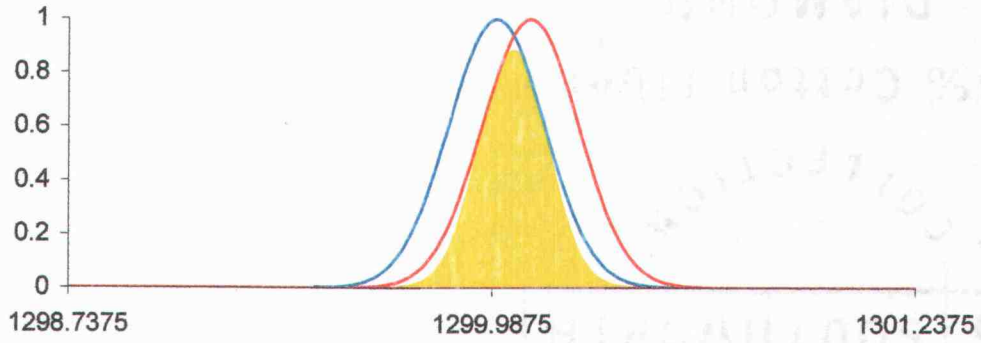

a)

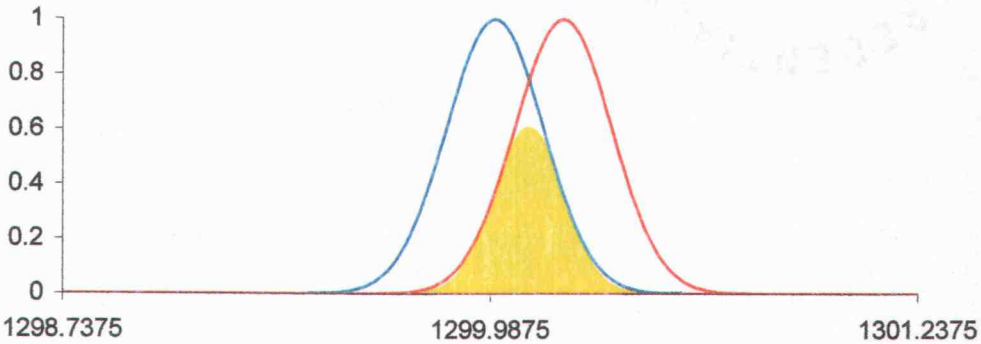

b)

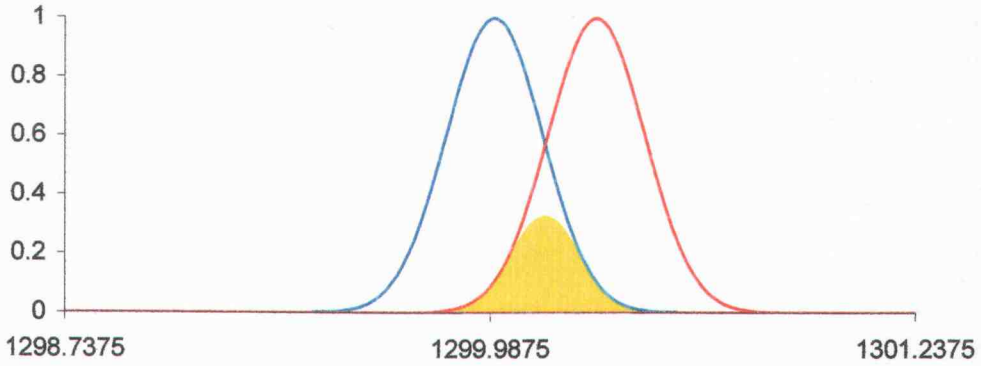

c)

Figures 1.3a-c Three plots showing change in reflected signal as a fiber grating is stretched in a fiber grating sensor system. The red curve illustrates the reflectivity profile of the stationary grating, the blue curve illustrates the strained grating, and the yellow shaded area illustrates the optical power that reflects off of both gratings and reaches the detector.

Other, more complicated approaches to FBG signal demodulation have been developed, including systems tailored to high speed demodulation [8] and demodulation of multiple gratings along one fiber [8, 9, 10 and 11]. One simple approach would be to use a tunable, narrow bandwidth fiber-coupled laser to replace the LED, one coupler, and one FBG in the setup. This would provide for a much stronger optical signal due to the greater light output of a laser over a narrow wavelength range and would also allow for the interrogation of multiple FBGs along one optical fiber.

1.2 Fiber Bragg grating inscription

Several methods of fiber Bragg grating inscription have been developed and published. All of the methods of inscribing an FBG involve the use of light to induce an index of refraction change, but vary in the mechanism used to create the periodic high and low regions of light intensity that cause an FBG to be formed. The method used to write the first FBGs will be discussed, followed by the two writing methods currently used to write gratings commercially and a fourth method used at OSU to write gratings.

1.2.1 Photosensitivity of optical fibers

Fiber Bragg grating inscription requires the ability to achieve a change in the index of refraction of the core of the fiber. To enable light guiding, the cores of

optical fibers are doped with a small percentage of germanium, which increases the index of refraction in the fiber core. The germanium in the core of the fiber also gives rise to photo-induced changes in the index of refraction; if the core of the fiber were pure fused silica, grating growth will not occur [4].

The photosensitivity in germanium-doped optical fibers arises from germanium-oxygen defect centers (GODCs) [13]. Regular SiO_2 and GeO_2 have one oxygen atom between each Ge or Si atom, as illustrated in Figures 1.4a and 1.4b. Sometimes, a weaker bond is formed between Ge and Si atoms, or between two Ge atoms, that lacks the intermediate oxygen atom (Figure 1.4c). This weaker bond requires 5.06 eV of energy to break, which lies within the ultraviolet range. As products of the photochemical reaction, a GeE′, SiO^{+}_{3} (or GeO^{+}_{3}) and e^{-} are created, and the absorption of light near 5.06 eV is reduced [14, 15 and 16].

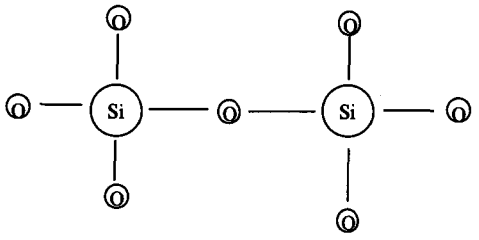

a)

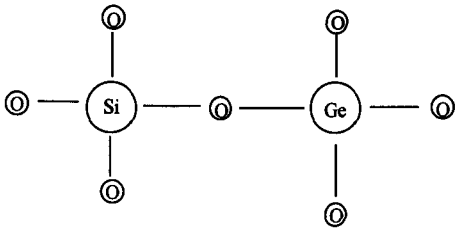

b)

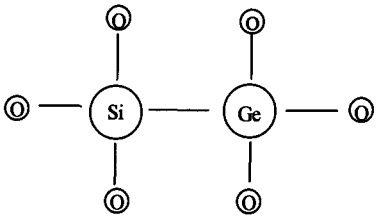

c)

Figures 1.4a-c Diagrams of the standard SiO_2 glass structure (a), Ge-Si structure that occurs in the fiber core as a result of Ge doping (b), and Ge-Si bond lacking the intermediate oxygen atom, a Germanium Oxygen Defect Center (c).

As a result of the reduction in light absorption near 5.06 eV, the index of refraction at longer wavelengths is changed slightly as calculated through the Kramers-Kronig relation [4]:

$$\Delta n_{eff}(\lambda') = \frac{1}{2\pi^2} P \int_0^{\infty} \frac{\Delta \alpha_{eff}(\lambda)}{1-(\lambda/\lambda')^2} d\lambda, \qquad (1.2)$$

where the change in index of refraction is calculated as an integral of the change in absorption, $\Delta\alpha_{eff}$ over all wavelengths. The application of the Kramers-Kronig relation relating change in absorption in the UV to change in index of refraction at the grating wavelength has been labeled the "color-center model." Other models have been developed to explain grating formation due to the densification of glass that occurs when using high power lasers and grating formation due to additional dopants in the fiber core [4, 17, 18, and 19].

Due to the low index change achievable in standard 3% germania telecommunication fibers such as Corning SMF-28, which typically exhibits index changes of ~$3x10^{-5}$, considerable research has been conducted to discover methods of increasing the photosensitivity of standard fibers [20,21]. The two easiest methods of increasing the photosensitivity of optical fibers are hydrogen loading and temperature treating. Co-doping the core is also possible, but requires special fiber to be fabricated. Hydrogen loading the fiber entails placing the optical fiber in a heated vessel that has been pressurized with hydrogen gas. Pressures ranging from 20 atm to 750 atm have been attempted at temperatures ranging from 20-75 °C, but typically a pressure of 150 atm is used [4]. The resulting increase in photosensitivity yields index changes of up to $6x10^{-3}$, a substantial improvement over non-hydrogen loaded fiber

[20]. Temperature treating the fiber is accomplished by heating the fiber using a flame, CO_2 laser, or any other method of producing high, localized temperatures. This method results in index changes of up to $1.75x10^{-3}$, while the same writing system was only able to achieve index changes of $1.6x10^{-4}$ in standard fiber. [21]

1.2.2 Internal Writing Method

Hill, Fujii, Johnson, and Kawasaki published the original paper on writing FBGs in 1978 [2]. The method used to write the original gratings has been termed the internal writing method. In the internal writing method, light from a laser source is coupled into an optical fiber with a cleaved end facet. The 4% reflection off of the cleaved end facet sets up a standing wave in the optical fiber, with periodic regions of high and low intensities, as illustrated in Figure 1.5. Regions of higher optical intensity undergo an index of refraction change, resulting in the formation of a periodic Bragg grating. The Hill paper used a 488nm argon ion laser, coupled into a one meter length of optical fiber to produce gratings with 90% reflectivity [2]. While relatively easy to achieve in the lab, the internal writing method has several characteristics which make it unsuitable for use in most grating applications. Gratings written using the internal writing method are limited to having reflectivities at wavelengths at or near the writing wavelength. As the writing wavelength must be near 480nm to allow for a two-photon absorption at the right energy to cause a change in index, gratings cannot be written at the low loss wavelength regions used for optical communications systems. Additionally, the index of refraction change due

to the two-photon absorption process is fairly small, requiring long gratings to produce high reflectivities [2].

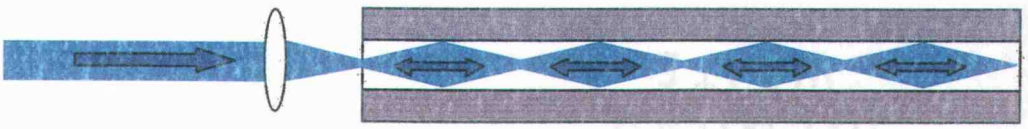

Figure 1.5 Schematic illustrating internal writing method by coupling light into the end of the fiber and relying on reflection from the end facet to set up a standing wave pattern. Note that the blue region in the fiber is not representative of the spatial distribution of the light in the fiber, but an illustration of the standing wave in light intensity.

1.2.3 Phase Mask Method

The phase mask method, shown on the next page in Figure 1.6, employs an optical phase mask, which is essentially a diffraction grating with grooves having a depth so that light traveling straight through a groove is one-half wavelength out of phase from light traveling straight through a ridge. This provides for strong cancellation of the 0^{th} order diffraction, so that a higher percentage of the incident light is concentrated in the +1 and –1 diffractive orders. In a region just after the phase mask, the +1 and –1 diffraction orders overlap due to the spatial extent of the laser beam. In this overlapping region, the two beams create an interference pattern so that if an optical fiber is placed in the overlapping region, an FBG can be written [22, 23].

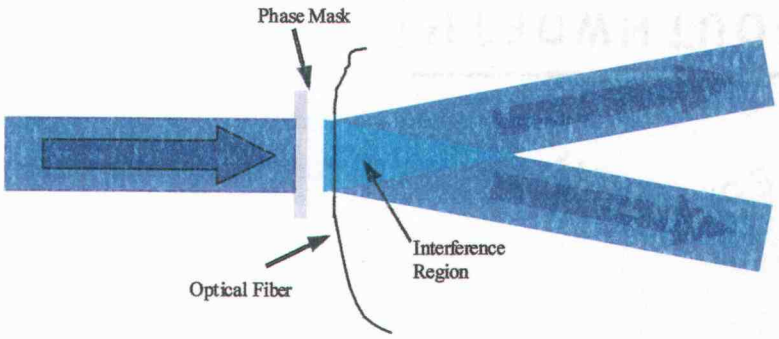

Figure 1.6 Schematic of phase mask method of FBG inscription, illustrating positioning of the fiber within the interference region after the phase mask.

The phase mask method is relatively easy to align and is the most stable of the transverse grating writing methods. Unfortunately, each phase mask can only write optical fiber gratings at one wavelength, which depends only on the ruling spacing of the phase mask [22]. Writing FBGs at different wavelengths requires another phase mask at a high cost.

1.2.4 Holographic Method

The transverse holographic method shown in Figure 1.7 was developed to allow optical fiber grating construction at various wavelengths using the same optical elements [24]. Instead of using a phase mask to split the writing laser into two beams, a 50:50 beamsplitter is employed. The beam that is transmitted through the

beamsplitter is reflected off of a mirror so that both beams experience the same number of reflections to minimize effects due to low spatial coherence and non-uniform beam profiles. The two beams then reflect off of mirrors angled so that both beams cross creating an interference region. If an optical fiber is placed in the interference region, an FBG is written at a wavelength that depends on the writing wavelength and the angle of beam incidence as given by the relation:

$$\lambda = \frac{n_{eff}\lambda_w}{\sin\theta}. \tag{1.3}$$

The grating wavelength, λ, depends only on the effective index of refraction in the optical fiber, n_{eff}, the writing wavelength of the laser, λ_w, and the sine of the half-angle between the interfering beams, θ [24]. Note that rotation of the mirrors allows the inscription of FBGs at various wavelengths, but the holographic method is less stable than the phase mask method and requires a laser with a long coherence length due to uneven path lengths.

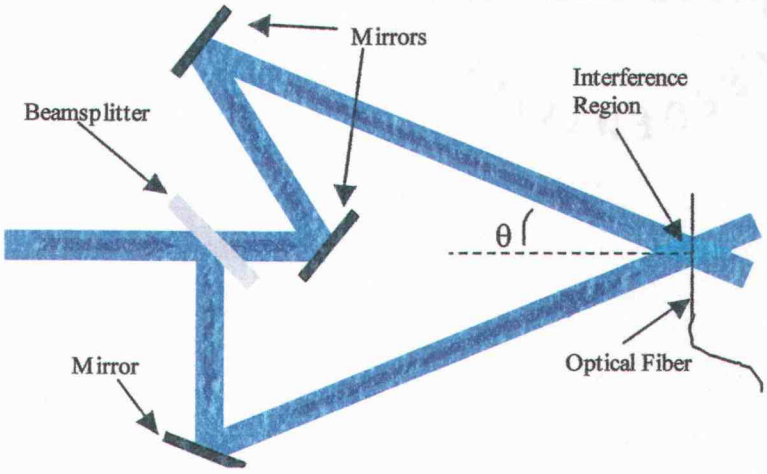

Figure 1.7 Schematic of transverse holographic method of fiber grating inscription. The beamsplitter, and three mirrors are employed to create an interference region which the optical fiber is placed in.

1.2.5 Modified Phase Mask

The modified phase mask method was developed to combine the stability of the phase mask method with the ability to write gratings at different wavelengths [25]. As shown in Figure 1.8, this method employs a phase mask to split the beams into +1 and –1 orders in a method similar to the phase mask method, but rather than place the fiber in the interference region after the phase mask, the +1 and –1 orders of light are sent onto two mirrors, then focused through a cylindrical lens onto the fiber [25, 26]. Rotation of the mirrors allows different wavelengths to be inscribed, and the 0^{th} order light that comes through the phase mask can be blocked. Both beams experience the same path length and the same number of reflections so that coherence

requirements are less for the modified phase mask method than the holographic method.

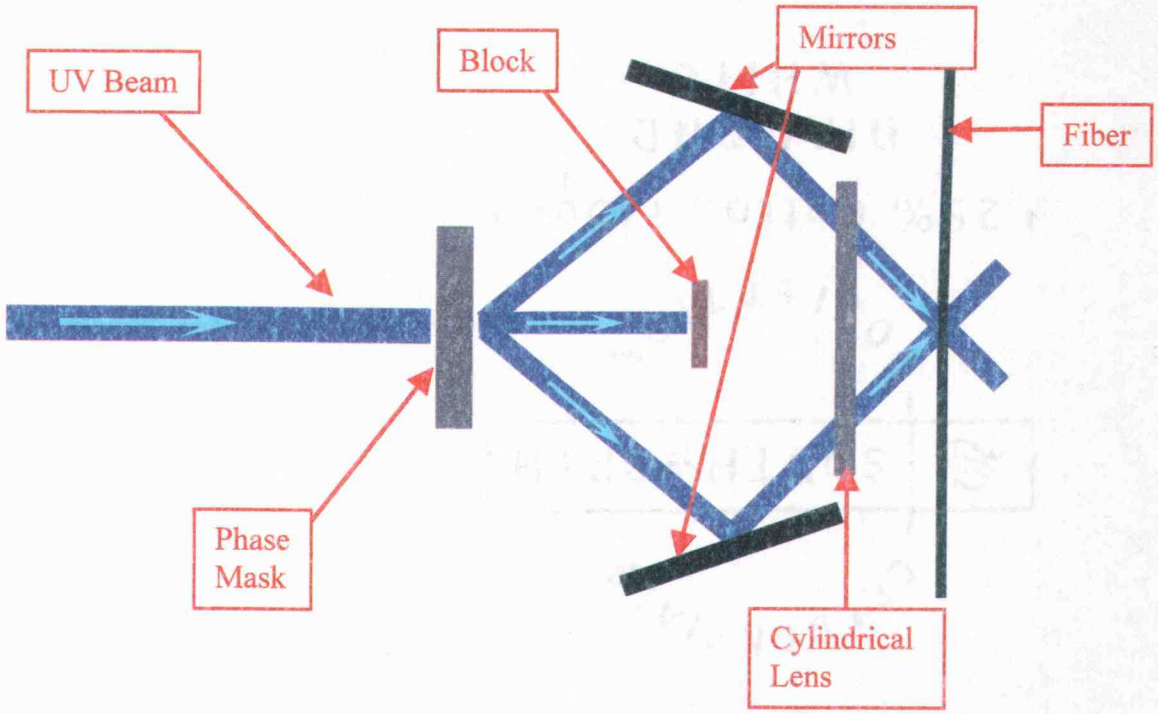

Figure 1.8 Schematic of modified phase mask method, illustrating positioning of the phase mask, beam block, mirrors, lens, and optical fiber.

1.2.6 Polyimide recoating

The removal of the epoxy acrylate or polyimide protective coating from a section of the optical fiber to allow grating inscription also allows the fiber to be easily damaged in the grating region. The epoxy acrylate and polyimide protective coatings

on optical fibers protect the fiber from water intrusion, micro cracks and other small damage that can lead to optical fiber breakage. To ensure durability of systems employing FBGs, it is necessary to recoat the stripped region of the fiber with a protective coating. Commercially produced gratings are typically available with the grating section recoated with polyimide. The recoating of gratings written at OSU is accomplished using a fiber recoating apparatus designed and constructed at OSU [27]. The fiber recoater, illustrated in Figure 1.9, consists of holders which position the optic fiber above two movable carts, one containing a small groove filled with polyimide to recoat the fiber, and another containing two heaters to cure the polyimide coating. To recoat the fiber, the fiber is placed in the apparatus, the first cart containing the polyimide filled groove is moved across the stripped section of fiber, coating it with polyimide, followed quickly by the second cart containing the heaters, which is left over the stripped section of the fiber for ten to fifteen minutes to cure the polyimide. This process is repeated three times to develop a coating at least 10 microns thick.

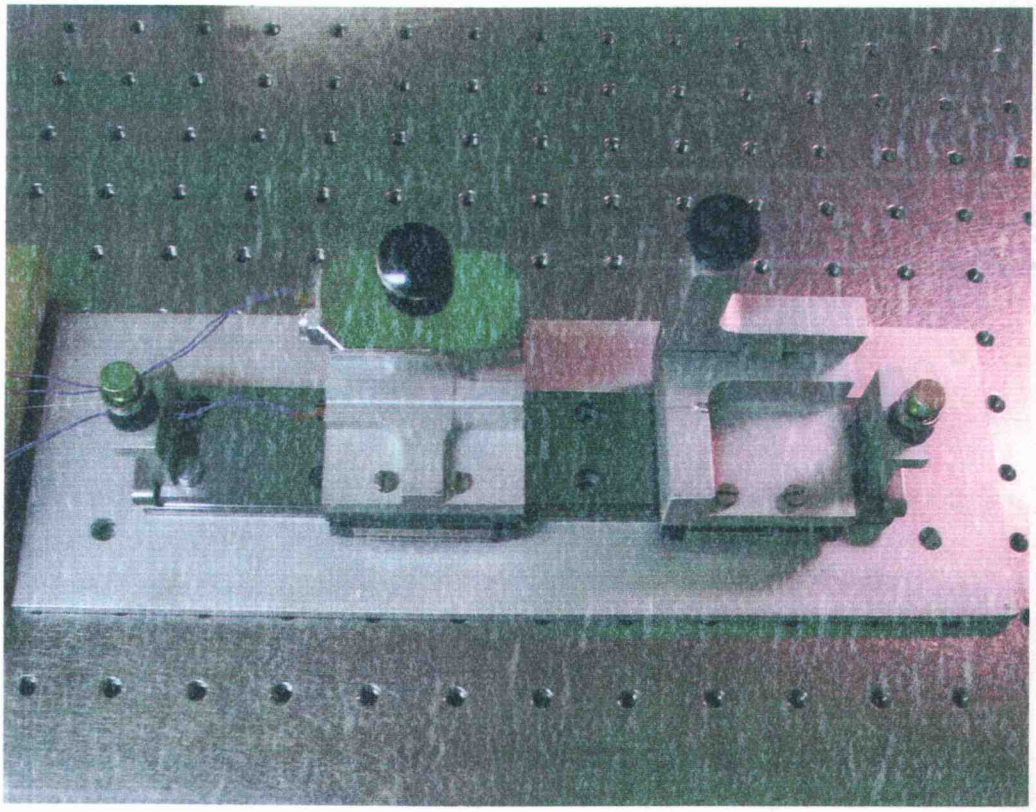

Figure 1.9 Photograph of optical fiber recoater. Optical fiber is held in place with clamps at either end, while the two movable sections are used to coat the fiber and temperature cure the polyimide. The section on the right is machined with a small groove to apply the polyimide coating, after which the left section, containing two cartridge heaters, is moved over the recoated section to cure the polyimide. The fiber is held in place by rubber clamps held down by the brass thumbscrews at either end.

Chapter Two

Diode laser characteristics

Due to their small size, low cost, and high efficiency, diode lasers are used in an amazing number of applications, from simple laser pointers and barcode scanners, to high bandwidth laser diodes for optical communication and high power laser diode arrays for pumping other complex laser systems. Because of this large array of varying applications of laser diodes, numerous different laser diode structures have been designed. This section presents a brief overview of a few different varieties of edge emitting laser diodes that could prove useful for fiber sensor systems.

2.1 Fabry-Perot diode lasers

Fabry-Perot diode lasers are the simplest laser diode structures, consisting of a semiconductor gain region with two cleaved end facets forming cavity mirrors. The optical power is confined within the gain region in the vertical direction due to total internal reflection from differing indices of refraction, and in the horizontal region by reflection from either carrier-induced index of refraction changes ("gain-guided" lasers), or static index of refraction changes due to the semiconductor structure ("index-guided" lasers). Index guided lasers confine the optical power in the gain

region much better than gain guided lasers, due to the larger index of refraction difference between the gain region and the surrounding semiconductor. This tighter optical confinement allows for a lower threshold laser diode [29].

Due to the large semiconductor gain bandwidth (20-50nm) and the close spacing (less than 1nm) of the Fabry-Perot cavity modes of the laser diode due to the length of the diode cavity, Fabry-Perot cavity laser diodes often lase on multiple longitudinal modes, as shown in the plot below, Figure 2.1. The cavity mode spacing $\Delta\lambda$ can be calculated at the wavelength of interest λ from the effective index of refraction n_{eff} and the length of the cavity L as follows [29]:

$$\Delta\lambda = \frac{\lambda^2}{2n_{eff}L} \tag{2.1}$$

Changes in temperature and injection current change which longitudinal modes of the laser will lase and can slightly shift the longitudinal modes.

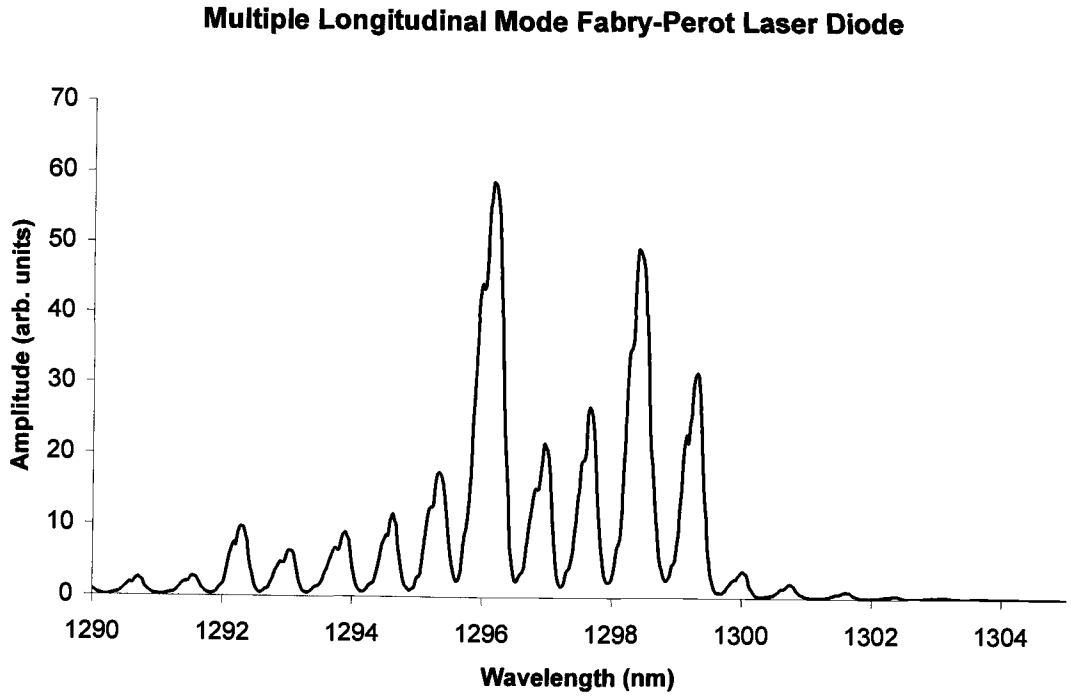

Figure 2.1 Output spectrum of nominally 1300nm multiple longitudinal mode Fabry-Perot laser diode.

2.2 Distributed Bragg reflector diode lasers

Distributed Bragg reflector (DBR) diode lasers are more complex structures than Fabry-Perot diode lasers. Instead of employing cleaved semiconductor facets for cavity reflectors, DBR lasers have Bragg reflectors formed in the semiconductor at both ends of the gain region. These Bragg reflectors consist of square or sinusoidal thickness variations of the semiconductor cladding materials and only reflect at one wavelength in the semiconductor gain width, forcing the laser to lase on only one wavelength [30]. This stabilizes the wavelength of the laser so that the laser wavelength does not change with changing injection current. A schematic illustrating

the arrangement of the Bragg reflectors and the gain medium is shown in Figure 2.2, below [28].

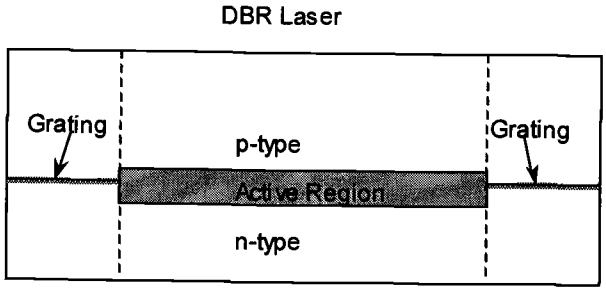

Figure 2.2 Schematic illustration of distributed Bragg reflector semiconductor laser. The distributed Bragg reflectors are located at the ends of the laser cavity, outside of the active region of the laser, and serve as narrow bandwidth reflectors forcing lasing to occur at the wavelength corresponding to the peak in reflection from the Bragg reflectors.

2.3 Distributed feedback lasers

Distributed feedback (DFB) lasers are similar to DBR lasers in their utilization of Bragg reflectors to stabilize the diode laser wavelength, but instead of using two separate Bragg reflectors outside of the gain region, DFB lasers employ a periodic Bragg structure spanning the length of the active region as shown in Figure 2.3 [28]. The period of the Bragg structure in the DFB laser is chosen so that the light in one laser mode is coupled between forward and backward propagating waves within the diode laser, causing only that laser mode to lase.

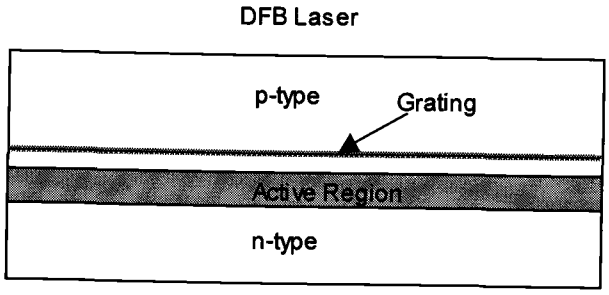

Figure 2.3 Schematic illustration of DFB semiconductor laser. The distributed feedback is caused by the grating and has strong wavelength dependence similar to an FBG so that only one wavelength within the gain region of the semiconductor lases.

2.4 Tuning of diode laser wavelengths

Research on several methods of tuning the emission wavelength of diode lasers has been conducted for over 20 years for uses in spectroscopy and other applications, but the major impetus behind tunable diode laser research, wavelength division multiplexing in optical communications systems, is a relatively recent development [12]. Wavelength division multiplexing in optical communications systems allows up to 160 different signals to travel down the same fiber by using up to 160 separate laser diodes, each operating at a slightly different wavelength, coupled into the same optical fiber. Since the different wavelengths of light do not interact with each other, the bandwidth of each optical fiber can be increased dramatically, but this method requires wavelength stable, single longitudinal mode lasers [31] and a complicated combining method to couple light from all of the lasers into the same optical fiber. DFB diode lasers possess the required wavelength stability and single longitudinal mode behavior and so are virtually exclusively used as sources in WDM optical

communication systems. Unfortunately, this requires a different laser diode to be stocked for each of the wavelengths used in a WDM system, and diminished network capacity in the event of a laser diode failure, until the failed laser diode can be manually replaced. A wavelength stable, tunable diode laser could replace the large inventory requirement and allow remote reconfiguring of WDM networks in the event of laser failure, or could help balance bandwidth demand when necessary [12].

2.4.1 Temperature tuning

Temperature tuning is one of the simplest methods for tuning diode lasers. Increasing or decreasing the temperature of a laser diode has two effects on the laser diode: it shifts the gain curve and alters the effective length of the cavity. As temperature is increased, the center of the gain curve shifts towards longer wavelengths. The thermal expansion and index change due to temperature combine to yield a larger effective cavity length as temperature is increased. In a Fabry-Perot laser diode, the change in length of the laser diode cavity changes the mode spacing slightly and continuously, while the change in the center wavelength of the gain curve causes the laser to jump from one mode to the next, resulting in a temperature dependence of approximately 0.5 nm/°C [28]. In a DFB or DBR laser diode, the lasing wavelength is controlled by the period of the grating structure so that thermal shifts in the gain curve center cannot shift the lasing wavelength. In this case, increasing temperature increases the effective spacing between index changes of the

Bragg grating in the laser diode both due to thermal expansion and thermo-optic effects, resulting in a wavelength shift of 0.09 nm/°C [28].

2.4.2 Injection current tuning

Injection current tuning naturally occurs in Fabry-Perot laser diode structures as the injection current is increased beyond threshold. In a Fabry-Perot laser diode, increasing the current causes the gain curve to shift towards shorter wavelengths, which, if isolated, would result in the laser hopping modes to shorter wavelengths. Due to increased energy dissipation in the laser diode at higher injection currents, thermal effects usually dominate so that modes at shorter wavelengths decrease in intensity and modes at longer wavelengths increase in intensity, resulting in an overall shift to longer wavelength of the laser output [30]. Unfortunately, as mentioned in Section 2.4.1 and shown in Figure 2.4, this shift is not continuous, but rather a trade-off between different modes of the Fabry-Perot cavity. The power output also changes substantially as the current is varied.

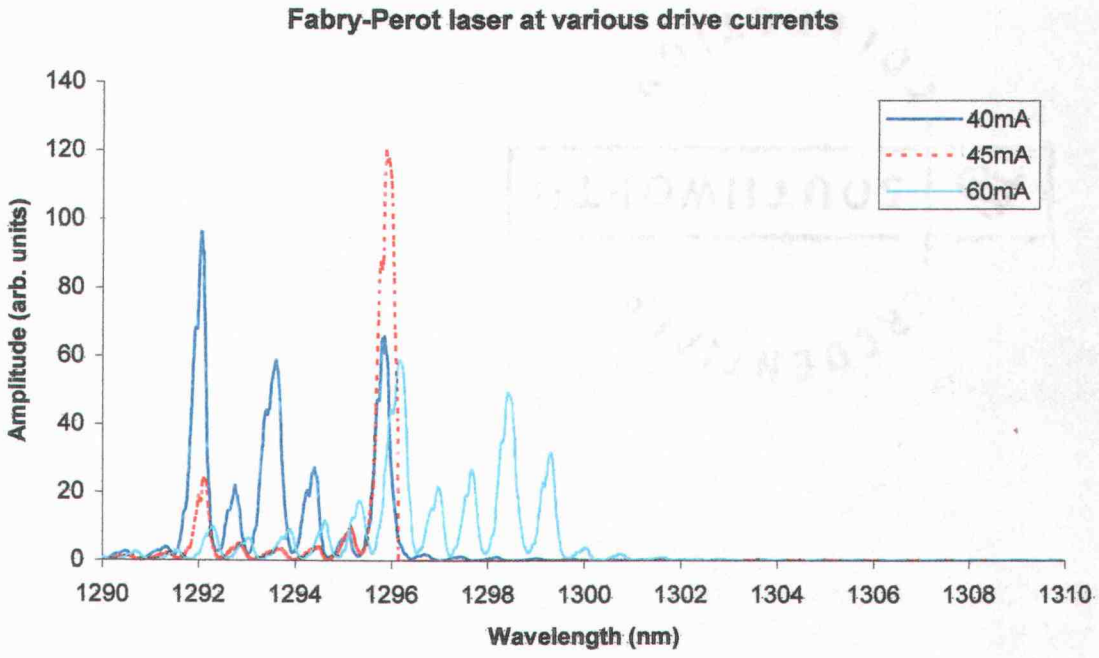

Figure 2.4 Plot illustrating wavelength shift of a 1300nm fiber-coupled Fabry-Perot diode laser to longer wavelengths as injection current is increased. Power outputs have been scaled separately to appear on the same graph.

Complex laser diode structures, such as multiple section DBR and coupled cavity lasers, can achieve more continuous tuning by injecting differing amounts of current into different sections of the laser. In a tunable DBR laser, current is injected into the Bragg reflector sections of the laser diode cavity, causing a change in reflected wavelength by changing the index of refraction in the Bragg reflector. An additional section located next to the gain section, between the Bragg reflectors, labeled the phase section in Figure 2.5 on the next page, is used for tuning the effective length of the laser diode cavity so that the wavelength reflected by the Bragg reflectors corresponds to a supported mode in the laser diode cavity. The tunable DBR laser

has the advantages of lasing on a single longitudinal mode due to the Bragg reflectors and separate control of the output amplitude and lasing wavelength [32]. Similar methods are used in coupled cavity laser devices.

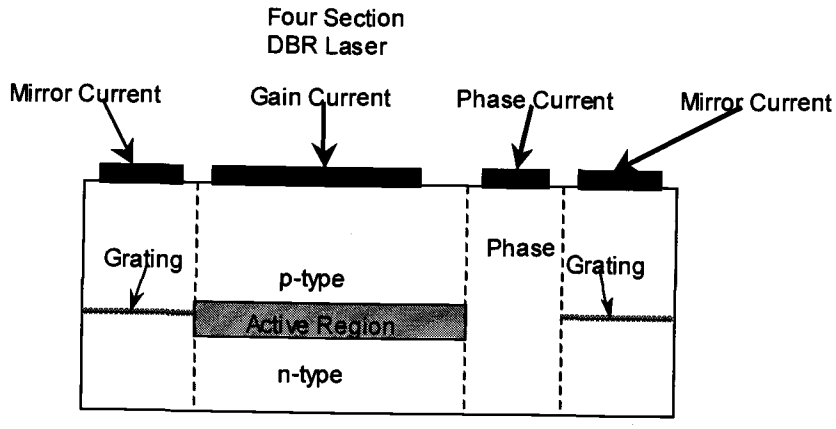

Figure 2.5 Structure diagram of a four-section wavelength tunable DBR laser diode illustrating separately injection current tuned gain, mirror, and phase sections. Diagram after [32].

2.4.3 External reflector

The addition of an external reflector to a Fabry-Perot laser diode can stabilize the output of the laser diode to one wavelength due to the overlap of modes of the laser diode and the external cavity formed by the reflector. Slightly changing the position of the external reflector changes the mode spacing of the external cavity and can be used to change which longitudinal mode of the laser diode corresponds to the modes of the external cavity, changing the operating wavelength of the laser diode. In this method, tuning is limited to discrete jumps equal to the mode spacing of the Fabry-Perot laser diode cavity [28]. Increasing the length of the laser cavity can

reduce the size of these longitudinal mode hops but will still not provide continuous tuning.

Another option employing external reflectors is the use of an external reflector as the output mirror on extremely short laser diode cavities only a few microns in length [12]. Due to the difficulty in constructing a standard waveguide laser only a few microns long, research on this method of laser tuning has focused on vertical cavity surface emitting lasers (VCSELs). Further difficulties lie in manufacturing VCSELs that operate at 1.55μm and obtaining large output powers from laser diodes of such short lengths. Typically, VCSELs employ distributed Bragg reflectors on their output facets to increase the cavity lifetime and thus increase the photon density within the cavity to promote lasing. In 2001, Nortel announced a tunable VCSEL employing an electrostatically movable mirror positioned at the output of the VCSEL, which is externally pumped by another laser diode to produce 20 mW of output power. Bandwidth9 also announced a tunable VCSEL employing a Bragg reflector on an electrostatically controlled torsion beam [12].

2.4.4 External reflection grating

An evolution of the external reflector approach is to employ a diffraction grating to reflect light of a particular wavelength back into a Fabry-Perot laser diode. Two standard methods of employing a diffraction grating for laser diode tuning are used, Littrow and Littman. Both methods are illustrated in Figure 2.6. In the Littrow configuration, the output beam from a laser diode is collimated using a lens

and directed upon a reflection grating oriented so that the –1 order of the desired wavelength is reflected back into the laser diode, with the 0^{th} order used as the output. The desired wavelength of operation is tuned by changing the angle of the grating. Unfortunately, this also changes the direction of the output beam, making this method difficult to implement in fiber-coupled systems. The Littman configuration employs both a diffraction grating and a mirror to avoid the output beam direction changes that occur in the Littrow configuration. In the Littman configuration, the laser beam is collimated using a lens and directed at grazing incidence on a diffraction grating, producing two beams, the 0^{th} order reflection from grazing incidence off of the diffraction grating, and another beam at a large angle to the grating surface. This beam is reflected back upon the diffraction grating through the use of a mirror. The operating wavelength is changed by changing the angle of the mirror reflecting light back on the grating, which changes the wavelength reflected back into the laser diode. Since the diffraction grating remains fixed, the direction of the output beam is unchanged.

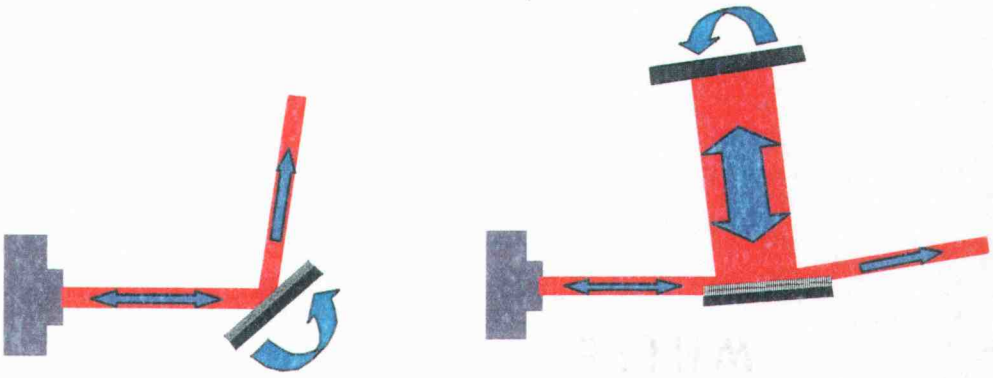

Littrow Configuration Littman Configuration

Figure 2.6 Diagram of Littrow and Littman configurations for tuning lasing wavelengths of diode lasers using reflection diffraction gratings. Curved arrow indicates which optical element is rotated to tune the lasing wavelength.

2.4.5 External fiber Bragg grating

In a method similar in concept to the external reflection grating methods, a Fabry-Perot laser diode can be optically coupled into a single-mode optical fiber containing an FBG. With this method, the FBG reflects one wavelength of light back into the laser diode, forcing the laser to lase on the wavelength reflected by the FBG, if the FBG is at a wavelength corresponding to the modes of the laser diode cavity [33]. Tuning is accomplished by stretching or compressing the FBG to shift the wavelength reflected by the FBG. As the wavelength reflected by the FBG changes, the intensity of the operating mode of the laser diode increases and the intensity of the next mode of the laser cavity increases, until the next mode is the lasing mode and

the previous mode is suppressed. As the possible lasing modes are still restricted by the Fabry-Perot modes of the laser cavity, this method of tuning is not continuous [34].

Chapter Three

Laser Diode Models

The computational modeling of physical systems is a common practice used to provide insight into the dynamics of physical systems. Computational modeling has been used to predict the results of an experiment before it is conducted, to analyze data from experiments using a theoretical model in an attempt to understand the underlying reasons behind the experimental results, and to predict behavior on scales currently beyond measuring capabilities. Modeling optical systems enables the prediction of the optical behavior of a system without requiring its actual construction. Several commercial optics modeling packages, such as Zemax and Code V, are currently available for the modeling and design of optical systems and lasers, but in some cases, commercial software does not provide the capabilities or flexibility necessary to model a desired system. Laser diode modeling software focuses on the design of the semiconductor layout of the laser diode and does not usually include the ability to include complex optical elements external to the laser diode. In modeling the AR-coated, FBG-coupled tunable laser diode system, the main focus of the model needs to be the external cavity and not the semiconductor layout, so it is necessary to write a computer program for the model rather than rely on a commercial optics modeling package.

Construction of a laser diode model requires a theoretical approach to the laser diode behavior using basic equations. Complete modeling of a laser diode involves calculation of mode structure and gain. There are two major methods of modeling external feedback on laser systems: the Lang-Kobayashi model and the coupled cavity model.

3.1 Lang-Kobayashi Model

The Lang-Kobayashi (L-K) model is the most widely used analysis method for modeling external feedback on laser diodes [35]. In the L-K model, a single longitudinal laser mode is assumed and a perturbation approximation applied to model the effects of external feedback on the single longitudinal mode [36]. One disadvantage of this method is the assumption of a single longitudinal mode, which is usually not the case for Fabry-Perot cavity laser diodes, as the spectrum shown in Figure 2.1 illustrates. To account for this limitation of the Lang-Kobayashi model, researchers have added multiple modes by adding an additional number of longitudinal modes all equally spaced, either through rate equations, or iterative schemes [35]. While this does allow for multiple longitudinal modes, it also requires assumptions to be made about the number of modes and the mode spacing. This method is unsuitable for use in modeling the AR-coated FBG-tuned laser diode since the effects from the feedback will be substantially larger than the effects from the diode cavity and the number of modes supported by the laser system is unknown.

There are two main equations in the basic Lang-Kobayashi model, one for the electric field of the single longitudinal mode, including gain, and another for the excess carrier density [36]. Multimode behavior is included by allowing a series of separate electric field equations and either a mode-dependent gain, or self- and cross-saturation processes to include mode interaction. Utilizing the mode-dependent gain method, the basic equations of the Lang-Kobayashi model become:

$$\frac{dE_m}{dt} = \frac{1}{2}(1+i\alpha)(G_m(N)-\gamma_m)E_m(t) + \frac{\kappa}{\tau_l}E_m(t-\tau)e^{(-i\omega_{0m}\tau)} + F_m(t) \tag{3.1}$$

and

$$\frac{dN}{dt} = \frac{I}{e} - \frac{N}{\tau_s} - \sum_{j=-M}^{M} G_m(N)|E_m|^2 . \tag{3.2}$$

[37, 38]. In Equations 3.1 and 3.2, E_m is the slowly varying electric field of the m^{th} mode, with nominal frequency ω_{0m}, excess carrier density N, gain G_m, injection current I, electron charge e, spontaneous carrier lifetime τ_s, Langevin noise force F_m for spontaneous emission, mode-dependent cavity loss γ_m, internal round trip time τ_l, and linewidth enhancement factor α. The last three are generally assumed equal for all modes. External feedback is included through the feedback level κ and external cavity round trip time τ. For further discussion of the Lang-Kobayashi model, see references 47 and 48, as well as 36, 37, and 38, previously cited.

3.2 Coupled Cavity Model

Lamb, Lang, and Scully originally developed the coupled cavity model in 1972 in an attempt to explain the narrow linewidth of lasers in a paper examining the interaction between the Fox-Li modes of the Fabry-Perot laser cavity and the lab environment by treating the laser as if it were a short region at one end of a long cavity, separated from the rest of the cavity by a partially transmitting window [39]. In 1983, Ebeling and Coldren applied this coupled cavity model to multi-element semiconductor lasers, modeling laser diodes that consist of two or more active gain regions which are created by etching a small gap in the gain region of a semiconductor laser diode [40]. Further work was conducted in 2000 by Pierce, Rees, and Spencer, using the coupled cavity model in combination with a complicated gain model to find chaotic regions of output in a laser diode with a uniformly reflecting external mirror [35]. In these last two cases, the advantage of not having to decide the lasing modes separately from the model is evident.

The coupled cavity model of a system is created by breaking the system down into separate regions for each dielectric section, as shown in Figure 3.1 on the next page.

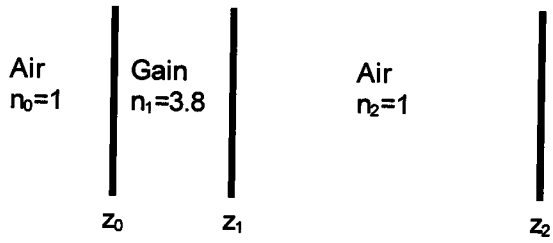

Figure 3.1 Illustration of the dielectric sections used in the coupled cavity model. Positions of index changes are labeled z_m with indices of refraction between the index changes as n_m. The illustrated schematic is for a simple Fabry-Perot laser operating in air.

Right and left traveling electric field amplitudes of the form:

$$E_m(z) = A_m e^{-ik_m z} + B_m e^{ik_m z} \tag{3.3}$$

are written for each of the dielectric sections m, where A_m and B_m are the complex field amplitudes and k_m is the complex propagation constant, given by the angular frequency of the light ω, the speed of light c, and the real and imaginary components of the index of refraction in the section n_m and κ_m, respectively [4]:

$$k_m = \frac{\omega}{c}(n_m + i\kappa_m). \tag{3.4}$$

The magnetic fields H_m can similarly be written as:

$$H_m(z) = -\frac{k_m c}{\omega} A_m e^{-ik_m z} + \frac{k_m c}{\omega} B_m e^{ik_m z}. \tag{3.5}$$

Boundary conditions at the boundaries of the dielectric layers z_m require the tangential components of E and H to be continuous. These boundary conditions can be expressed using matrix notation and used to write matrices to couple field amplitudes between the dielectric sections:

$$\begin{pmatrix} A_{m+1} \\ B_{m+1} \end{pmatrix} = Q(z_m) \begin{pmatrix} A_m \\ B_m \end{pmatrix} \tag{3.6}$$

with the Q matrix at z_m as:

$$Q(z_m) = \begin{pmatrix} \frac{k_{m+1}+k_m}{2k_{m+1}} e^{i(k_{m+1}-k_m)z_m} & \frac{k_{m+1}-k_m}{2k_{m+1}} e^{i(k_{m+1}+k_m)z_m} \\ \frac{k_{m+1}-k_m}{2k_{m+1}} e^{-i(k_{m+1}+k_m)z_m} & \frac{k_{m+1}+k_m}{2k_{m+1}} e^{-i(k_{m+1}-k_m)z_m} \end{pmatrix}. \tag{3.7}$$

For a coupled cavity system with a given number of separate regions (M, below), the same number of Q matrices exist. Applying each of these Q matrices in series to the field amplitudes at the left end of the cavity yields values for the field amplitudes at the right end of the cavity:

$$\begin{pmatrix} A_{M+1} \\ B_{M+1} \end{pmatrix} = Q(z_M)Q(z_{M-1})\ldots Q(z_0) \begin{pmatrix} A_0 \\ B_0 \end{pmatrix} \tag{3.8}$$

Additionally, since the laser diode is not externally optically pumped, the incoming field amplitudes for the left (B_0) and right (A_{M+1}) sides of the cavity must equal zero:

$$\begin{pmatrix} 0 \\ B_{M+1} \end{pmatrix} = Q(z_M)Q(z_{M-1})..Q(z_0)\begin{pmatrix} A_0 \\ 0 \end{pmatrix}. \tag{3.9}$$

This constraint on incoming fields requires that the Q_{11} component of the Q matrix be zero so that despite the complex appearance of the above equations, with a given cavity design, there is only one independent variable, the complex propagation constant k_l [35]. The other propagation constants can be written in terms of k_l using the values for the index of refraction in each section of the laser. By breaking k_l into its real and complex components, as in Equation 3.4, above, the constraint on incoming fields can be used to calculate the complex component of k_l at a given value for the real component of k_l. The complex component of k_l yields the gain threshold for the cavity mode corresponding to the chosen real component. From the threshold gain values, cavity lifetimes can be determined, as will be shown in the next section.

Cavity lifetimes are values for the average lifetime of a photon in the laser cavity. Photons are lost from the cavity via two mechanisms, scattering and output through the end mirrors. The two lifetimes add inversely, as the photons can leave the cavity through either mechanism:

$$\frac{1}{\tau_l} = \frac{1}{\tau_l^{mirror}} + \frac{1}{\tau^{scatt.}}. \tag{3.10}$$

The scattering lifetime is assumed to be the same for all wavelengths of interest in the laser diode model, due to the narrow range of wavelengths calculated

[40]. The mirror lifetimes can be calculated by a simple ratio of the energy stored in the cavity and the amount of energy lost through the end faces of the cavity:

$$\tau_l^{mirror} = \frac{Electromagnetic\ energy\ stored\ in\ system}{Energy\ lost\ through\ output\ per\ unit\ time} \tag{3.11}$$

The energy stored in the system is calculated by summation over the energy in each of the sections in the cavity:

$$\sum_{m=1}^{M} \int_{z_{m-1}}^{z_m} \langle U_m(z) \rangle dz, \tag{3.12}$$

while the energy output through the cavity ends is calculated by summing the energy flux through the two end faces:

$$2\sqrt{\frac{\varepsilon_0}{\mu_0}}\left(\eta_0 |A_0|^2 + \eta_{M+1} |B_{M+1}|^2\right), \tag{3.13}$$

where η_i is the index of refraction of the i^{th} section. The total expression for the mirror lifetime is then given by [35]:

$$\tau_{mirror} = \frac{\sum_{m=1}^{M} \int_{z_{m-1}}^{z_m} \langle U_m(z) \rangle dz}{2\sqrt{\frac{\varepsilon_0}{\mu_0}}\left(\eta_0 |A_0|^2 + \eta_{M+1} |B_{M+1}|^2\right)}. \tag{3.14}$$

With the cavity lifetimes calculated, a series of equations for the carrier density and photon density can be calculated.

Carrier density in the gain region changes due to three effects. Injection current directly increases the carrier density, while both spontaneous and stimulated emission provide for loss of carriers. Combining these three effects yields the following equation for the carrier density in the gain region:

$$\frac{dN}{dt} = \frac{J}{qd} - \frac{N}{\tau_{sp}} - \sum_l g_l S_l . \tag{3.15}$$

J is the injection current density in units of current/area, while d is the thickness of the gain region, so that J/d is the volumetric charge density injected into the gain region per unit time. Dividing by the electronic charge, q, yields the injected carrier density. The second term on the right hand side accounts for carrier loss through spontaneous emission, which depends only on the total carrier density N and the spontaneous recombination lifetime τ_{sp}, so that N/τ_{sp} is the number of carriers that spontaneously decay per unit time. The summation term is a sum over all of the different wavelengths (or modes, l) within the region of interest. Each mode has a

different gain (g_l) and photon density (S_l) associated with it, so that the product $g_l S_l$ yields the loss of carriers due to gain at that particular mode. Summing over all of the modes yields the loss of carriers due to stimulated emission [35].

The photon density in the gain region of the laser cavity is affected by three terms in a manner similar to the carrier density. Photons are created by either spontaneous emission, or stimulated emission, and leave by either scattering or output through the end mirrors. The equation for the photon density in each of the modes of interest is:

$$\frac{dS_l}{dt} = \frac{\Gamma \gamma N}{\tau_{sp}} + \Gamma g_l S_l - \frac{S_l}{\tau_l} . \qquad (3.16)$$

This equation must be calculated separately for each mode of interest in the laser system, so that if ten different wavelengths are studied, ten photon density equations exist. The first term on the right hand side accounts for spontaneous decay of carriers. In the carrier density equation, above, the spontaneous decay term was simply N/τ_{sp}, which includes all carriers that spontaneously decay. Of the carriers that spontaneously decay, only a fraction (γ) of the emitted photons will remain within the laser cavity. The confinement factor, Γ, accounts for the evanescent field that extends beyond the gain region of the cavity. That is, if there are S photons in the cavity, there will only be ΓS photons within the gain region, so that the increase in photon density due to stimulated emission is $\Gamma g_l S_l$. Finally, photons are lost through either

scattering or output through the end mirrors. Since the two lifetimes for scattering and mirror output were combined using Equation 3.10, this term is simply S/τ.

The carrier density and photon density equations are each applied to the carrier density and photon densities iteratively until the turn on transients have decayed if steady-state operation is to be studied, or until the desired time has passed, if examining turn-on behavior. Once this has been done, the output spectrum is calculated from the photon density as the optical power in each mode:

$$P_{out_l} = \frac{\hbar c k_l V S_l}{\tau_l^{mirror}}, \tag{3.17}$$

with V as the volume of the gain region.

Chapter Four

Continuously tunable fiber Bragg grating coupled diode laser

Section 2.4.5 of Chapter 2 discussed tunable external cavity diode lasers employing FBGs as wavelength selective mirrors. Tuning in these devices is accomplished by applying strain or compression to the FBG but is not continuous due to the Fabry-Perot modes of the diode laser cavity. If the front facet of the diode laser is antireflection coated, the wavelength tuning accomplished by the FBG should no longer be limited to those wavelengths corresponding to the Fabry-Perot modes of the laser cavity, allowing continuous tuning of the laser diode operating wavelength. Construction of an antireflection coated, FBG coupled laser diode device allows direct observation of the output spectra which will enable comparison of the coupled cavity model with an actual device. Doug Ericksen, an M.S. Degree candidate in the Electrical and Computer Engineering Department at OSU, has conducted work on such a device as part of his thesis work. For this laser device, low cost 1320nm Fabry-Perot laser diodes were antireflection coated, mounted, and coupled into an FBG, and the output spectra measured.

4.1 Antireflection coating

The laser diodes used in this experiment were manufactured by Mitsubishi and packaged in a sealed TO-3 style package, requiring the removal of the laser diode can before antireflection (AR) coating. Once the can was removed, the length of the laser diode cavity was measured using a microscope and found to be 300 microns in length. The longitudinal mode spacing of the laser diode while under operation, 0.75nm at a nominal center wavelength of 1320nm, was measured using a Hewlett-Packard 70951A optical spectrum analyzer. Using this information and Equation 4.1, the effective index of refraction of the laser diode was calculated to be 3.8, which is approximately 5% higher than the generally accepted value of 3.6.

$$n = \frac{\lambda^2}{2L \cdot \Delta\lambda} \tag{4.1}$$

Ideal single layer antireflection coatings for air-material interfaces have an index of refraction equal to the square root of the index of refraction of the material, and a thickness equal to ¼ of the wavelength of the light in the material used for the AR coating. For the laser diodes used in this experiment, an index of refraction of approximately 1.95, with a thickness of 166.7 nm is nearly ideal. SiO, with an index of refraction near 1.9 was chosen for evaporation onto the laser diode to produce the AR coating. Unfortunately, thin film measurements of several evaporation samples

determined the index of refraction of the evaporated SiO film to be 1.7, requiring a slightly thicker coating of 194nm to reach the ¼ wavelength thickness. This lower index of refraction is most likely due to the film being oxygen rich.

A Veeco thermal evaporation system was used to antireflection coat the laser diode, with a Maxtek crystal thickness monitor used to monitor the amount of material deposited on the laser diode. Initial attempts to deposit an AR coating using only the crystal thickness monitor produced less than desirable results. The lasing threshold was not increased and, in some cases was actually reduced. To allow monitoring of the laser diode during the coating process, three additional electrical vacuum feedthroughs were added to the Veeco system, allowing the laser diode to be operated during the evaporation, and the output power of the laser diode measured using the photodetector built into the laser diode package. Using this method, material was evaporated onto the front facet of the laser diode until the lasing threshold reached a maximum, and the output power at a given current was minimal. Light output versus current (L-I) curves for the laser diode both before and after antireflection coating are plotted in Figure 4.1. Note that the output of the antireflection-coated laser diode is reduced by a factor of five at 25mA compared with the bare laser diode.

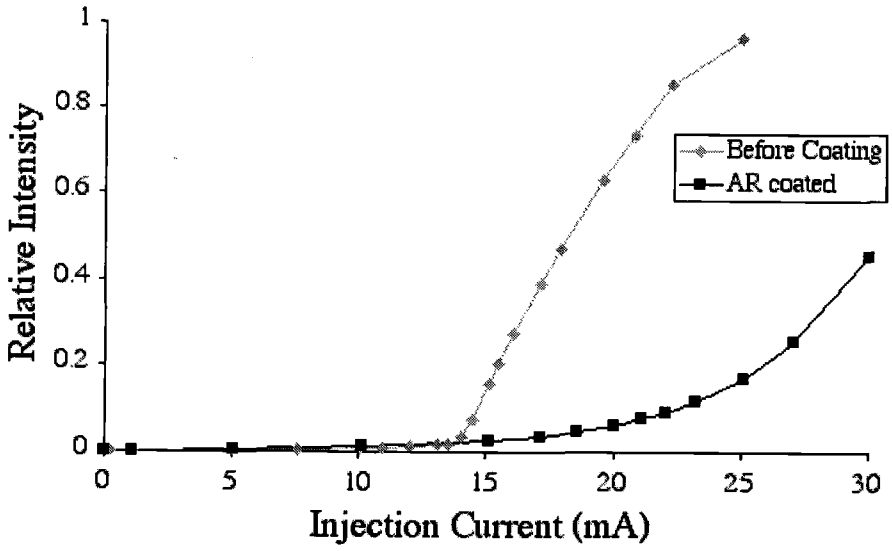

Figure 4.1 L-I curves for a laser diode both before and after AR-coating.

Spectra of the 1320nm laser diode were measured both before and after the antireflection coating process on the optical spectrum analyzer and appear in Figure 4.2. Of particular interest is the large shift in emission wavelength from 1315nm to 1290nm, most likely due to an increase in the number of carriers in the excited state.

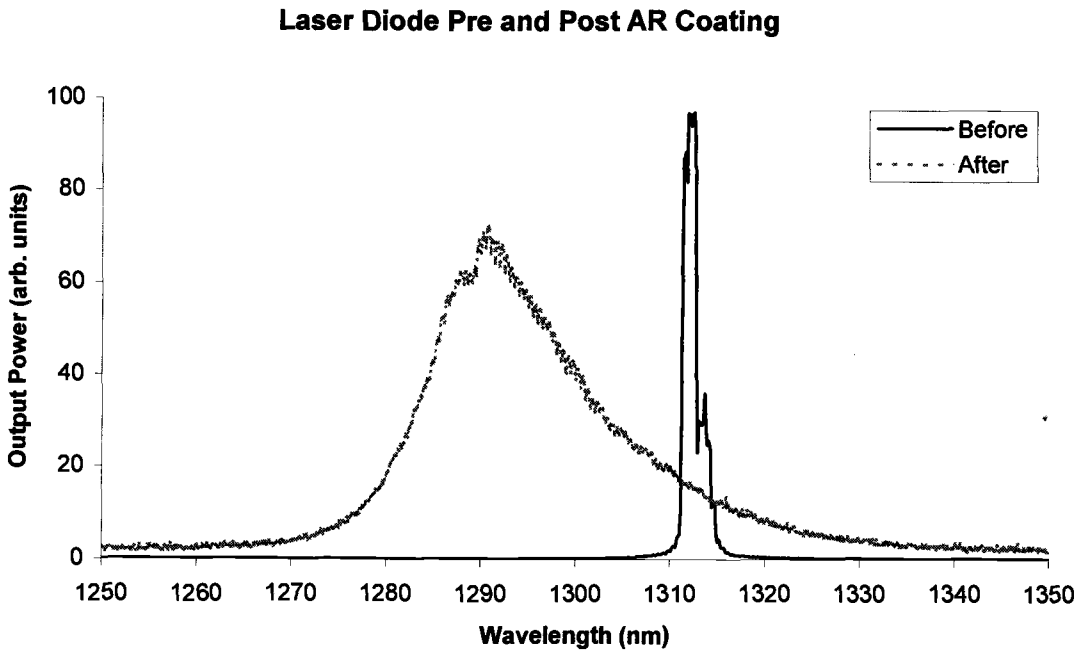

Figure 4.2 Plot illustrating shift in peak emission wavelength and broadening of emission of an antireflection coated laser diode. Both plots were generated at a laser drive current of 25mA, but have been scaled separately to appear on the same plot.

An ideal antireflection coating would yield a smooth output spectrum similar to an LED, without any ripple due to cavity modes [41]. A single layer antireflection coating produces 0% reflection at only one wavelength and only if the index of the coating is equal to the square root of the index of the substrate material. Due to the difference between the ideal index of refraction for the antireflection coating of 1.9 and the actual index of the applied SiO coating of 1.7, 0% reflection is unachievable and some cavity mode ripple is visible in the output of the coated diode. This ripple is unobservable in Figure 4.2 due to a lack of horizontal resolution, but taking a

separate scan using a narrower wavelength range on the OSA with a higher resolution allows the ripple to be seen, as shown in Figure 4.3.

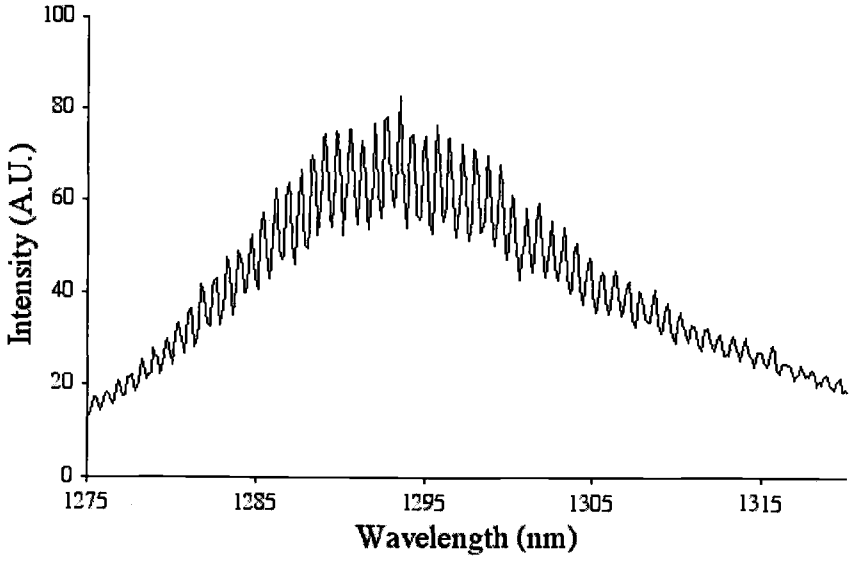

Figure 4.3 Output spectrum of SiO antireflection-coated laser diode, illustrating ripple in output due to laser cavity modes.

4.2 Grating construction for use with tunable laser

To ensure optimal tuning range, FBGs were written in hydrogen-loaded single mode Corning SMF-28 fiber with peak reflectivity wavelengths near the peak emission intensity from the antireflection coated laser diodes. The FBGs were constructed in-house at Oregon State University using the modified phase mask method described in Chapter 2. Figure 4.4 shows the FBG reflection spectrum superimposed on the emission spectrum of an antireflection-coated laser diode.

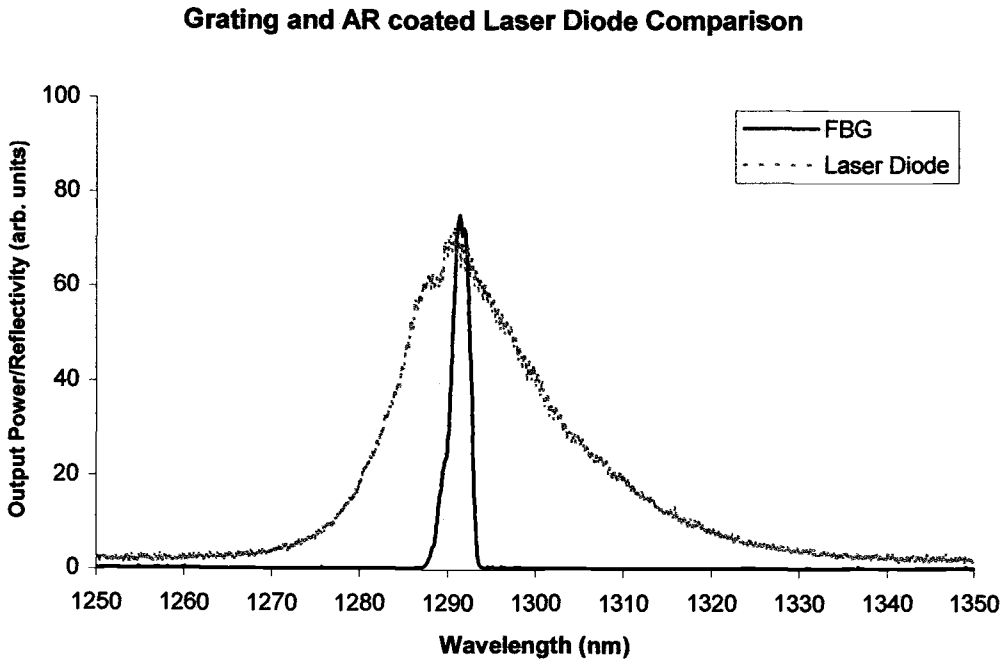

Figure 4.4 Plot illustrating reflectivity spectrum of FBG superimposed on emiss`ion spectrum of antireflection-coated laser diode.

4.3 Optical coupling

Due to the small output region of the laser diode (less than 1x10 μm), and the small diameter of the optical fiber core (9 μm), efficient coupling of light from the laser diode into the fiber requires that the optical fiber be placed as close to the end of the laser as possible without damaging the end of the laser diode. Additionally, the cleaved end of the optical fiber was lensed using a Fujikura optical fiber fusion splicer to improve the coupling into the core of the fiber. Coupling and alignment was initially conducted using a micrometer-adjusted xyzθφ fiber stage from Newport Optics, while looking through a microscope to position the end of the fiber as close as

possible to the laser diode. After initial experiments were conducted, a Newport single mode optical fiber alignment system employing piezoelectric actuators for fine tuning was made available through loan from Network Elements and was used to improve the optical fiber-laser diode coupling.

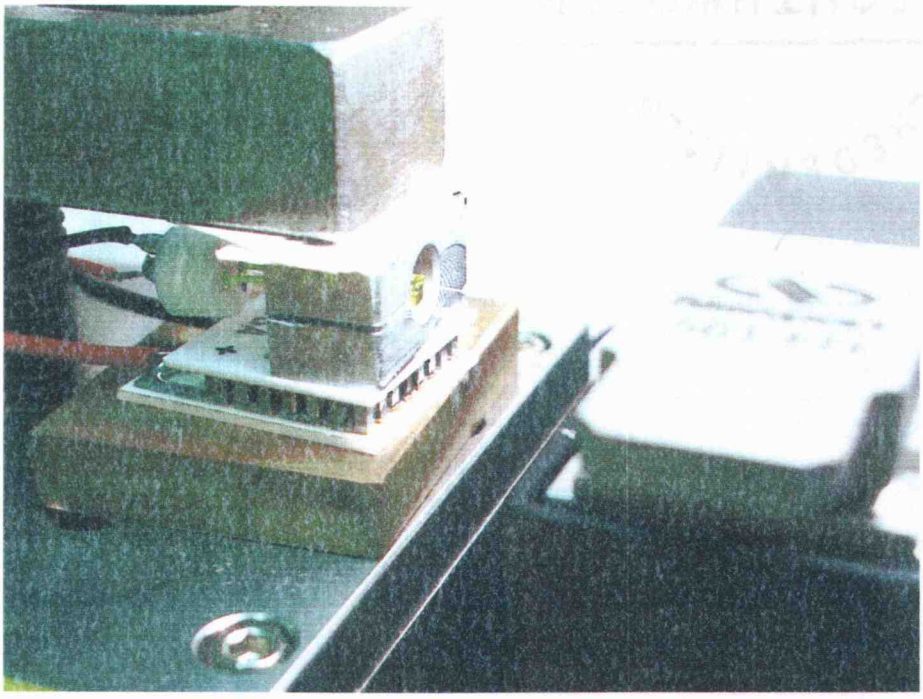

Figure 4.5 Picture of laser diode coupled into optical fiber, showing fiber holder, laser diode, heatsink, and thermoelectric cooler.

4.4 Wavelength tuning

Tuning of the lasing wavelength of the AR-coated laser diode was accomplished by applying longitudinal strain to the optical fiber grating. As mentioned previously, the optical fiber grating was written at a wavelength slightly smaller than the center wavelength of the laser output. After fabrication, the FBG was fastened to a micrometer adjustable translation stage using cyanoacrylate adhesive

so that adjustment of the micrometer applied a longitudinal tensile strain to the optical fiber. This arrangement allowed tuning of the FBG center wavelength over a range of 15nm, but to reduce chances of the optical fiber slipping through the adhesive or breaking, the FBG center wavelength was only tuned 10nm. Other tuning mechanisms have been reported that allow tuning over a range of 90nm using both tension and compression[42], a range that would easily allow tuning over the entire gain bandwidth of the laser diode.

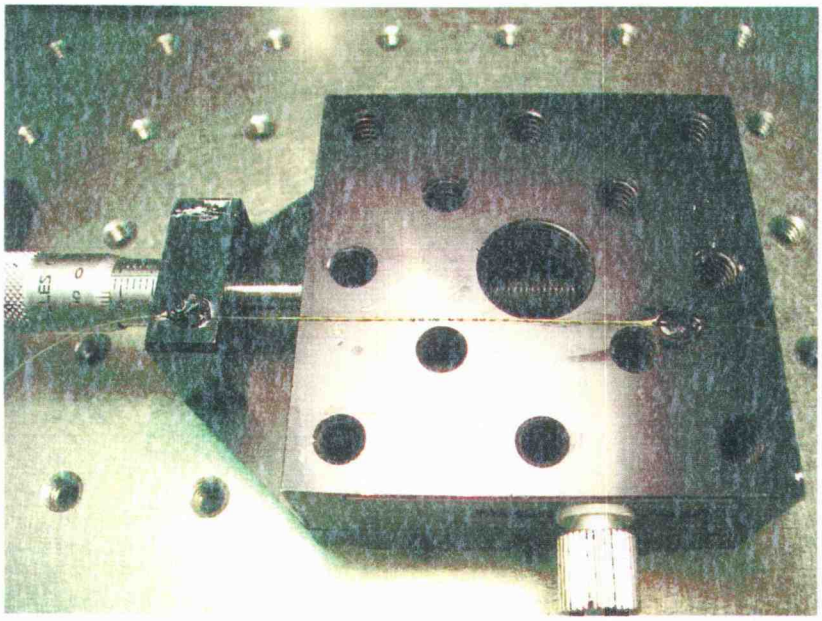

Figure 4.6 Picture of optical fiber grating attached to translation stage with cyanoacrylate adhesive to allow tuning of FBG center wavelength.

4.5 Output spectra

Output spectra for the AR-coated, FBG-coupled tunable laser device were taken with both a carefully aligned and a slightly misaligned fiber and are shown in Figure 4.7. When the fiber is misaligned with the laser diode, the amount of light reflected off of the FBG and returning to the laser cavity is insufficient to allow lasing and the output spectra appears similar to that of the bare AR-coated laser diode shown in Figure 4.3, but with the light reflected by the FBG removed from the output. Near optimal alignment, the amount of light reflected off of the FBG and returning to the laser cavity becomes sufficient to induce lasing at the same wavelength as the FBG, so that the output spectrum becomes that of a laser with a single longitudinal mode.

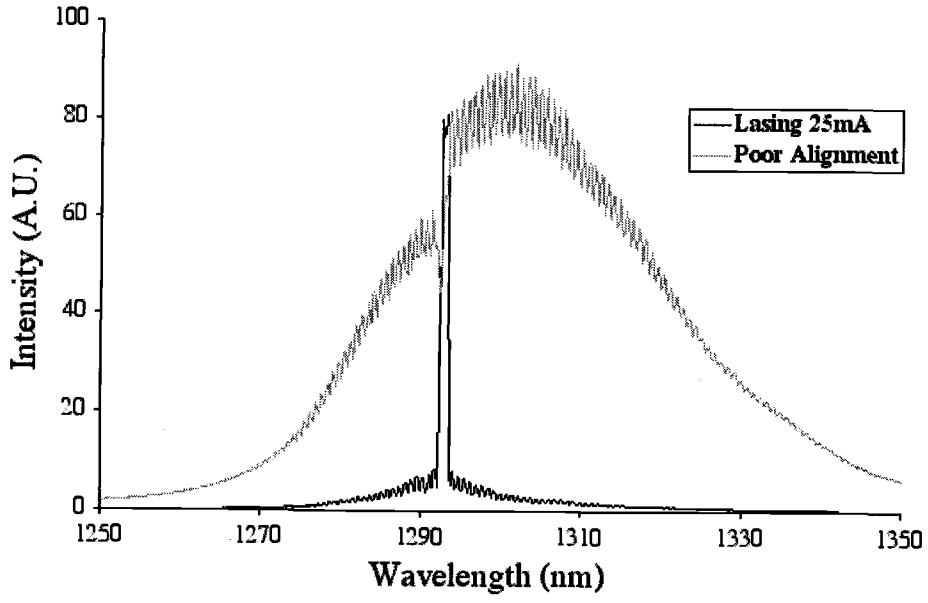

Figure 4.7 Output spectrum of FBG-coupled antireflection-coated laser diode device with both slightly misaligned and near optimal alignment. Output amplitudes are scaled separately to appear on the same graph.

Once the laser and FBG are aligned as accurately as possible by maximizing optical throughput, and lasing has been achieved, the FBG center wavelength is tuned using the translation stage method described in Section 4.4. Due to the residual effects of the original laser diode cavity present, continuous tuning is not achieved. As the FBG center wavelength is shifted, the single mode output of the laser diode decreases in intensity while at the same time lasing intensity increases at the wavelength corresponding to the next nearest mode of the original 300 micron long laser diode, so that the tuning is not continuous, but jumps from one longitudinal mode of the laser diode to the next, as shown in Figure 4.8.

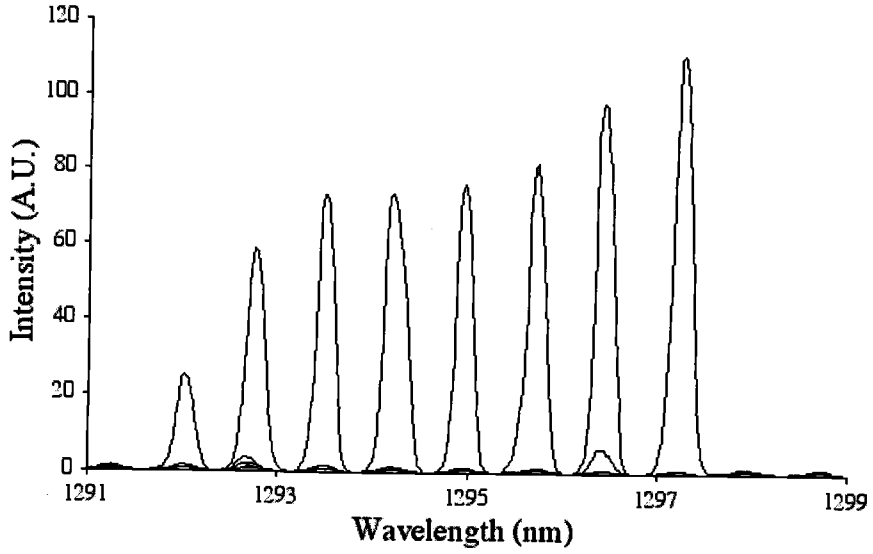

Figure 4.8 Output spectra of FBG-coupled antireflection-coated laser device at eight different levels of applied strain to the FBG. The first peak, at 1292 nm is with the grating unstrained, with longer wavelengths corresponding to increasing grating strain. Mode separation is approximately 0.75 nm.

Chapter Five

Computational model of FBG tuned laser diode

The FBG tuned laser diode described in Chapter 3 provides a new application for the coupled cavity laser model. To model the behavior of the FBG tuned laser diode and calculate expected output spectra, a computational coupled cavity model of the FBG tuned laser diode was developed. The model consists of a standard Fabry-Perot laser diode gain section with the ability to add additional dielectric sections outside of the gain section and was written in the computer language C++. This computational model closely follows the coupled cavity model described in Section 3.2. Microsoft Visual C++ was employed as the compiler with an additional library, the GSL 1.2 mathematical library, employed for complex number arithmetic. Separate C routines were written to calculate the absolute value of the 1,1 component of the complex matrix Q, solve for the minimum in Q, calculate photon lifetimes, carrier densities, gain, and photon densities. The main C program was used to tie these routines together in a process to calculate the output spectrum. The model was verified by calculating output spectra for both a regular and an AR-coated Fabry-Perot laser diode before being used to calculate output spectra for the FBG coupled laser diode.

5.1 Coupled cavity external reflector adaptation

The basic coupled cavity model described in Chapter three was applied to diode lasers to allow computation of the output of multi-section laser diodes [40]. An adaptation to the coupled cavity model that allows an external reflector of fixed reflectivity was developed by Pierce, Rees, and Spencer [35]. To include an external reflector, a step in the index of refraction with a value of:

$$n_{refl} = \frac{1+\sqrt{R_{ext}}}{1-\sqrt{R_{ext}}} \tag{5.1}$$

was included at the end of the optical cavity, assuming an air gap between the laser diode and the reflector [35]. This method is easily implemented into the standard coupled cavity model, but has several limitations. As physical constraints, the reflector must occur at the end of the laser cavity under consideration and have a reflectivity less than one. Additionally, due to the method used in [35] to calculate the index step, the index of refraction before the reflector must be one to yield the correct index step, and the reflectivity must be uniform over all wavelengths of interest. For the FBG-coupled laser diode, the first two limitations are unimportant, but the method needed to be altered to allow the section before the mirror to have an index of refraction larger than one and to allow a strong wavelength dependence on reflectivity. A re-derivation of Equation 5.1 using an arbitrary index of refraction before the reflective element yields:

$$n_{refl} = \frac{n_{prev}\left(1+\sqrt{R}\right)}{1-\sqrt{R}} \tag{5.1}$$

Wavelength dependence of the reflector was included by making the index of refraction a function of wavelength, rather than a constant value. A schematic representation of the laser diode cavity similar to Figure 3.1, but including each dielectric section for the AR coated FBG coupled laser diode is shown below, in Figure 5.1.

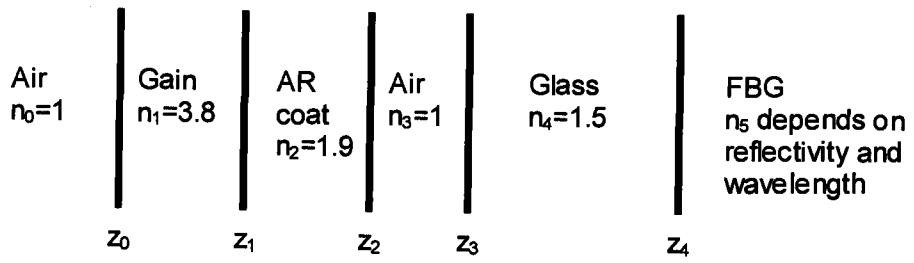

Figure 5.1 Illustration of the dielectric sections used in the coupled cavity model of the AR coated FBG laser diode. Positions of index changes are labeled z_m with indices of refraction between the index changes as n_m.

5.2 Q calculation

As described in Section 3.2 and enumerated in Equations 3.3-3.17, the assumption of a solitary laser operating allows two constraints to be made, which lead to the requirement that the 1,1 component of the Q matrix for the entire laser cavity must equal zero. To calculate this element, a series of matrices were set up in the computer, one for each section of the laser cavity. The matrices were multiplied together and the complex absolute value of the 1,1 component of the resulting matrix was calculated and returned as the result of the function.

5.3 Numerical solvers

Applying the constraint on the 1,1 component of the Q matrix requires the ability to solve for the complex value of the wavevector k that minimizes the value of the $Q_{1,1}$ component, given a real value of k. Two methods were used to find this value. First, a bracketing method was used to ensure that the minimum was trapped between known values of k, then a minimizing routine was employed to find the actual minimum. Brent's method of bracketing, as discussed in [43] was employed for the bracketing routine, with the modification of using complex functions and varying the complex component of a variable. A modified golden search routine, also from [43] was used to precisely calculate the actual minimum.

5.4 Photon lifetime

The photon lifetime is a measure of how fast light leaves the laser cavity and as previously mentioned, is a sum of two effects, scattering, and output through the cavity ends. The scattering lifetime of the photon is approximately equal for all wavelengths near the lasing wavelength and is taken to be 3.4 ps, after [40]. The lifetime due to output through the cavity ends is calculated using the coupled cavity model.

The imaginary component of the k wavevector is directly related to the gain or attenuation of the light wave. The value of k that satisfies the constraints on the

1,1 component of the Q matrix yields the threshold gain for the laser cavity at the given wavelength. This threshold gain can be employed to calculate the photon lifetime for a photon exiting the cavity through one of the end mirrors (Equation 3.14). Once the threshold gain has been calculated, each individual Q matrix is applied in turn to the right hand column vector (1,0), yielding relative photon densities in each section. From these relative photon densities, the relative energy density in each section is calculated and divided by the energy flux through the two end mirrors of the cavity to yield the photon lifetime due to cavity output. The two lifetimes, scattering and cavity, are combined using Equation 3.10. Figure 5.1, below, shows the wavelength dependence of the cavity lifetime for a 300 micron long optical cavity with an index of refraction of 3.8. Note that the spacing between the points of peak amplitude is about 0.7 nm, which agrees with the measured value given in Section 4.1.

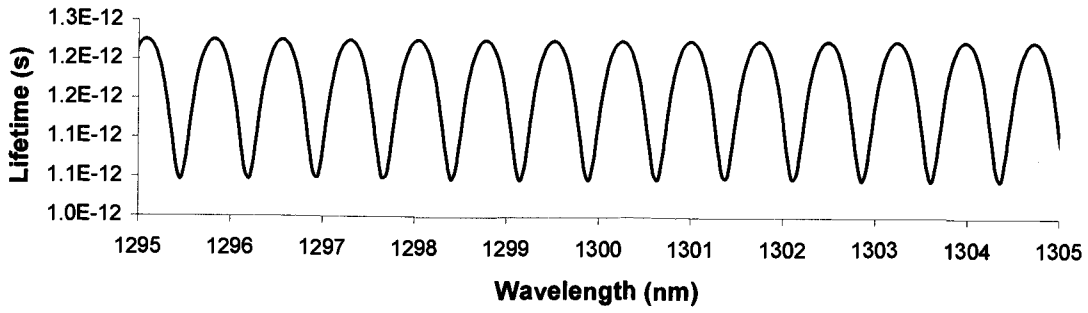

Figure 5.2 Plot illustrating the calculated cavity lifetime as a function of wavelength for a bare Fabry-Perot laser diode 300 microns long.

5.5 Carrier density

Calculation of the carrier density is accomplished using a straightforward approach of dividing the given injection current by the length, width, and thickness of the gain region and subtracting off the carriers due to spontaneous and stimulated emission. The gain region was taken to be 300 microns long, 10 microns wide, and .1 micron thick. These are typical measurements for the geometry of a Fabry-Perot laser diode and agree with measured values for the length and width of the 1320nm laser diodes used to create the external cavity laser described in Chapter 4. Spontaneous recombination time was taken to be 3 ns, after [30, 35].

5.6 Gain profile

The wavelength dependence of the gain profile was modeled by a parabolic equation after [28]. The general form of the parabolic gain profile equation is:

$$G(N,\lambda) = A(N - N_0) - B(\lambda - \lambda_0)^2, \tag{5.2}$$

The first term in the parabolic gain profile calculates the gain at the gain center wavelength, $\lambda=\lambda_0$. A is taken to be $2\text{x}10^{-6}$ $\text{cm}^{-3}\text{s}^{-1}$, and N_0, the carrier density to bias to transparency, is $4.5\text{x}10^{17}$ cm^{-3} [40]. The second term accounts for the falloff of the gain at wavelengths other than the peak gain wavelength. Center wavelength, λ_0, was set at 1300nm, and the B coefficient was set at $2\text{x}10^{9}$ $\mu\text{m}^{-2}\text{s}^{-1}$ [40]

5.7 Photon density

A separate photon density equation (Equation 3.16) is calculated for each of the 800 different wavelengths calculated in the program. The calculation of the photon density requires knowledge or assumption of several parameters. Γ, the confinement factor, was chosen to be 0.75 due to the strong mode guiding provided by double heterostructure lasers and through comparison of the output of the laser diode model at varying levels of Γ. Smaller values of Γ represent less confinement within the gain region and result in larger threshold currents and lower output power at a given injection current. The spontaneous emission factor, γ, the fraction of the spontaneously decaying light that is emitted into cavity modes, was taken to be 10^{-4}, after [40], and depends only on the cavity geometry, while the spontaneous emission lifetime, τ_{sp}, is the same as the spontaneous recombination time for carriers, 3 ns.

5.8 Main program

Actual model computations were conducted by running a main program that calls all of the separate routines in the proper order to calculate the output spectra. The number of sections of the laser, antireflection coating thicknesses and indices of refraction, lengths of fiber, and other important criteria of the laser cavity were read in to the program or entered before compilation. Grating reflectivity spectra were read in from a text file as a list of 800 separate reflectivities, one for each wavelength under study. Once these initial parameters were read in or entered into the program, the

main program calculates the index of refraction of the last section at each wavelength to provide the correct reflectivity. The $Q_{1,1}$ component of each of the 800 different wavelengths is then minimized using the numerical solvers and the imaginary component of k_i for each real value of k_i is recorded into an 800 element array. These values are then used in the photon lifetime calculations to yield the photon lifetimes for each of the wavelengths under study. Once the photon lifetimes have been calculated, the gain profile, carrier densities and photon densities are calculated recursively over each time step until 10 ns has passed, to avoid laser turn-on transients. The photon densities are then calculated for an additional time period and averaged to minimize effects from temporal fluctuations or ripple, in the output spectrum. The final output is calculated from the photon densities and mirror lifetimes by employing Equation 3.17.

5.9 Simulated Fabry-Perot laser diode spectrum

Validity of the laser diode model was checked by examining the calculated output spectra of a bare Fabry-Perot laser diode operating at several different levels of injection current. Output spectra were also calculated for several different time step values at an injection current of 25 mA. Larger time step values require fewer computations to reach the 10 ns time period and result in a faster running program, but also result in less accurate calculations. Calculation of the output spectra for several time step values allowed determination of a reasonable time step, as illustrated in Figure 5.2. One picosecond and one-hundred femtosecond time steps are too large

and produce unreasonable output spectra, while 10 fs, 1 fs, and 100 as time steps produce accurate output spectra. Due to the similarity between the three time step sizes that produce correct output, the largest time step of the three (10 fs) was chosen to minimize computation time. This time step results in a program which takes approximately one hour to run on an Intel Pentium 3 computer system running at 850MHz or one-half hour to run on an AMD Athlon 3.2GHz computer system.

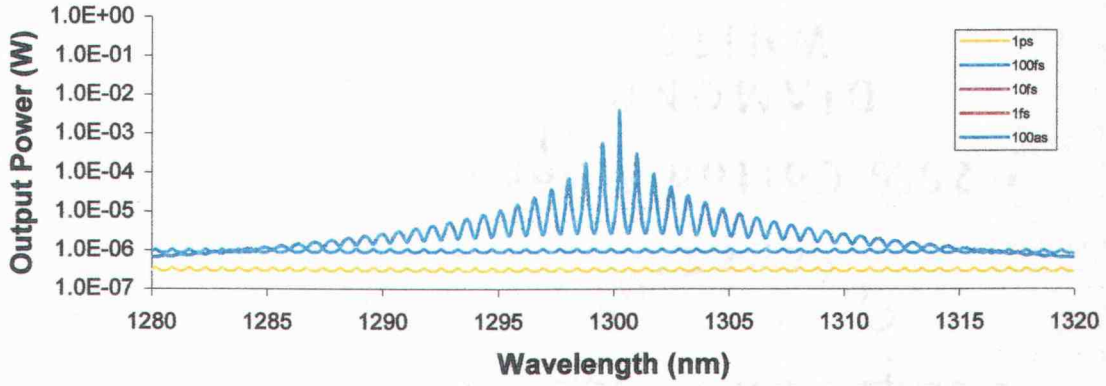

Figure 5.3 Plot illustrating calculated output spectra on a logarithmic scale for various time step values. 100as, 1fs, and 10fs plots are virtually indistinguishable, while the 100fs and 1ps plots are noticeably different.

Correct modeling of the laser diode output as a function of injection current was examined by calculating output spectra for fifteen different current levels from 0 to 60 mA. Peak output power was plotted as a function of injection current to examine the turn-on behavior of the laser diode as shown in Figure 5.3. Individual spectra were examined at each drive current and compared with typical laser spectra at the same drive current to ensure that the laser model accurately followed typical laser diode behavior—at low currents, output was similar to an LED, with cavity ripple.

Increasing current yielded a laser whose central modes gained amplitude as current was further increased, resulting in a narrower output spectrum. This is illustrated in Figure 5.4, which shows calculated output spectra for a laser diode operating both below and above lasing threshold.

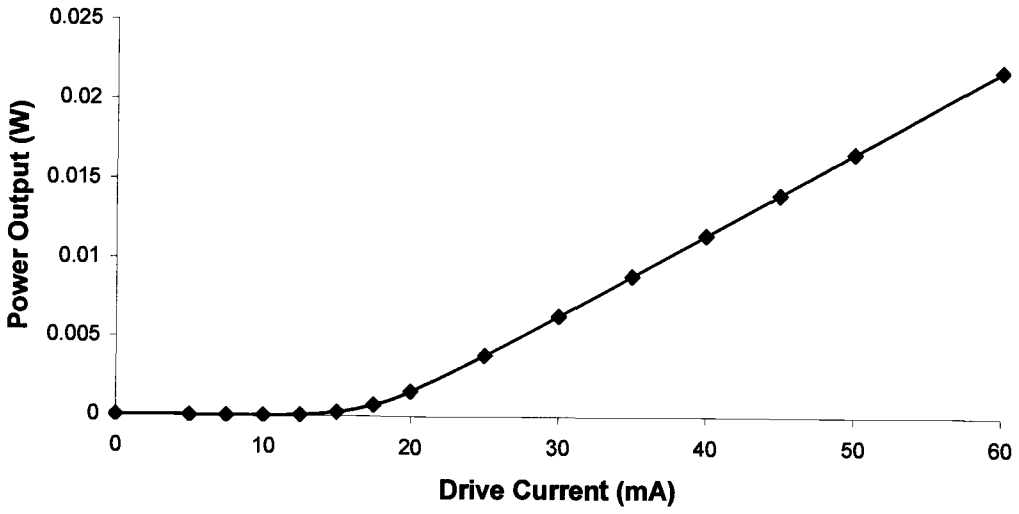

Figure 5.4 Plot illustrating calculated power output as a function of injection current for 15 different values of injection current.

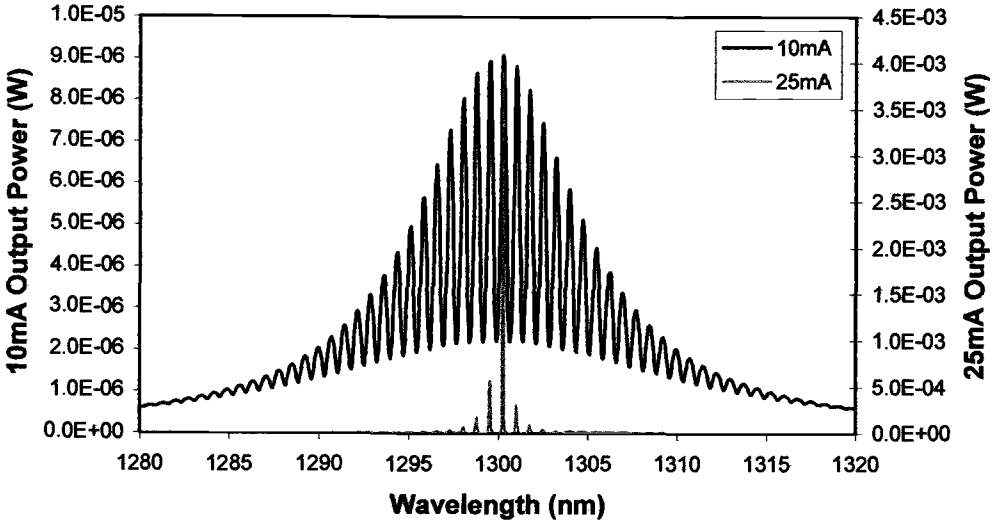

Figure 5.5 Plot illustrating calculated output spectra of a Fabry-Perot laser diode operating just below threshold (10 mA) and above lasing threshold (25 mA).

5.10 Simulated AR-coated laser diode spectrum

Antireflection coatings are added on the face of laser diodes as layers of dielectrics of certain thicknesses and indices of refraction. The actual laser diode used in the laser system described in Chapter 4 was antireflection coated with a single layer of silicon monoxide. Output spectra were calculated for a 300 μm long laser diode of effective index 3.8 with a single coating of 172 nm and an index of refraction of 1.9, near the ideal coating for a substrate index of 3.8 and similar to the coating applied to the laser in Chapter 4. At a drive current of 25 mA, the previous operating current of the physical laser diode and approximately twice the threshold current of both the laser model and actual laser diode, the antireflection coated laser diode is no longer

lasing, as shown in Figure 5.5, but still exhibits output ripple due to residual cavity modes.

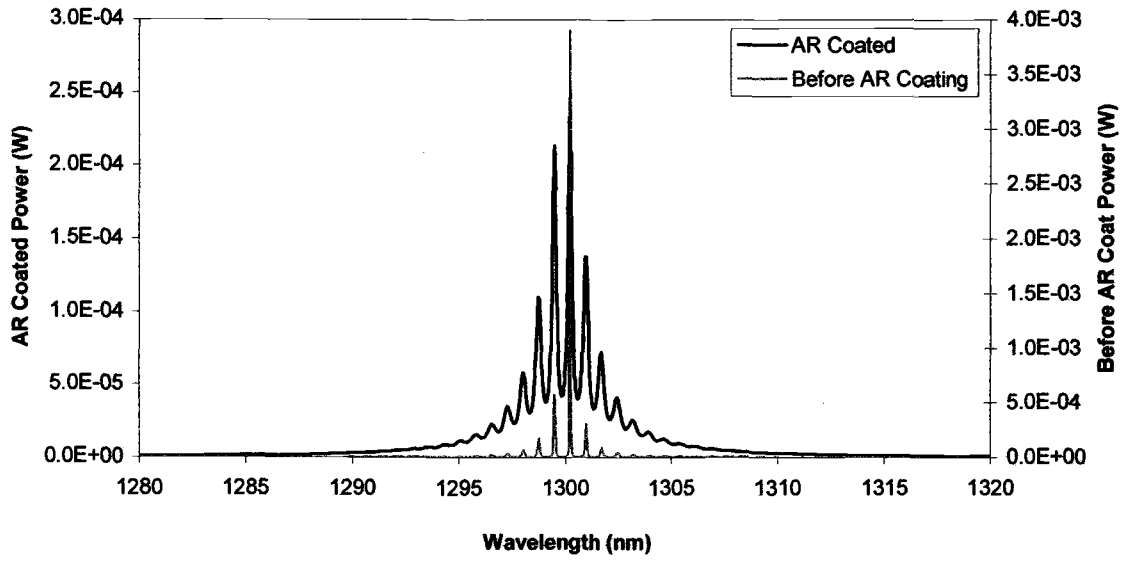

Figure 5.6 Plot illustrating calculated output of laser diode before and after anti-reflection coating with a single layer coating of 172nm of material with index of refraction of 1.9. Injection current is 25mA for both cases.

Output spectra for the antireflection coated laser diode were also calculated for an ideal single layer antireflection coating. Following the calculations in Section 4.1, the ideal single layer antireflection coating for a laser diode operating at 1300nm with an effective index of refraction of 3.8 is a layer 166.7nm thick of material with an index of refraction of 1.95. As discussed in Section 4.1 and [41], this ideal coating should produce an output spectrum without any output ripple from residual cavity modes. As shown in Figure 5.6, at a drive current of 25mA, no periodic ripple is present in the calculated output spectrum.

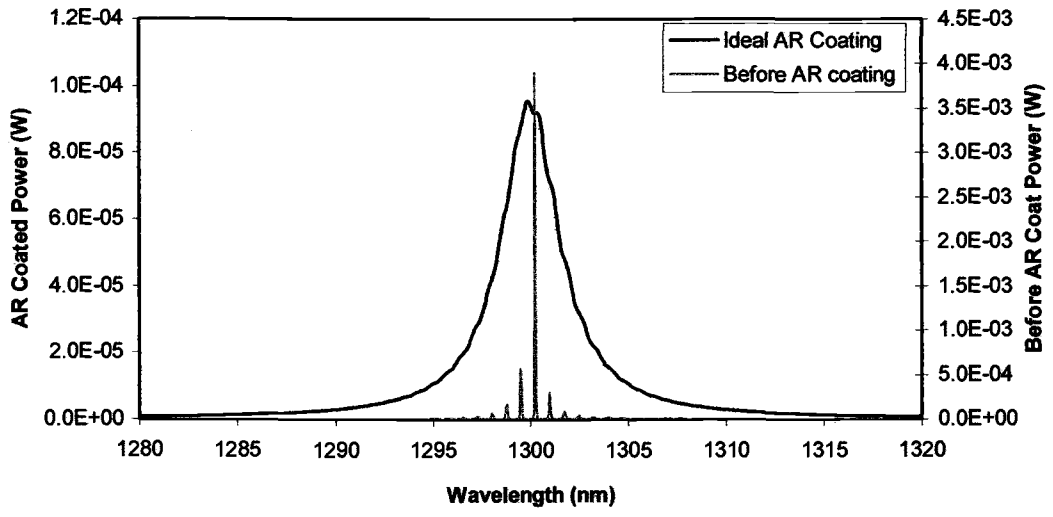

Figure 5.7 Plot illustrating calculated output of laser diode before and after anti-reflection coating with an ideal single layer coating of 166.7nm of material with index of refraction of 1.95. Injection current is 25mA for both cases.

5.11 Simulated AR-coated FBG-coupled laser diode spectrum

Once reasonable calculated output behavior was observed for both the bare laser diode below and above threshold and the AR-coated laser diode, output spectra of the AR-coated fiber Bragg grating coupled laser diode were calculated using a computer-generated Gaussian peak to represent a 30% reflective FBG. Output spectra were calculated at 25 mA injection current for several different wavelengths of FBG to represent straining the FBG in an actual FBG-coupled laser. Figures 5.7 and 5.8a-d illustrate output spectra at several different FBG center wavelengths. Figure 5.7 is linearly scaled to show that the side modes are of a low enough amplitude to be virtually invisible on a linear scale. Figures 5.8a-d are logarithmically scaled to allow

observation of side mode behavior. Note the small amplitude ripple visible in the logarithmically scaled output spectra well away from FBG center wavelength. This ripple has a period of approximately 0.75 nm and corresponds to the longitudinal cavity mode spacing of the original, bare laser diode. A higher amplitude, closely spaced ripple near the center wavelength of the grating corresponds to the longitudinal modes of the external FBG cavity. On close examination it is apparent that these peaks are actually two sets of closely spaced ripples of slightly different mode spacing superimposed on top of each other. Also, the center wavelength of the light output is not always at the same wavelength as the peak in the FBG, but can be pulled in either direction, due to the residual effects of the original 300 μm laser cavity.

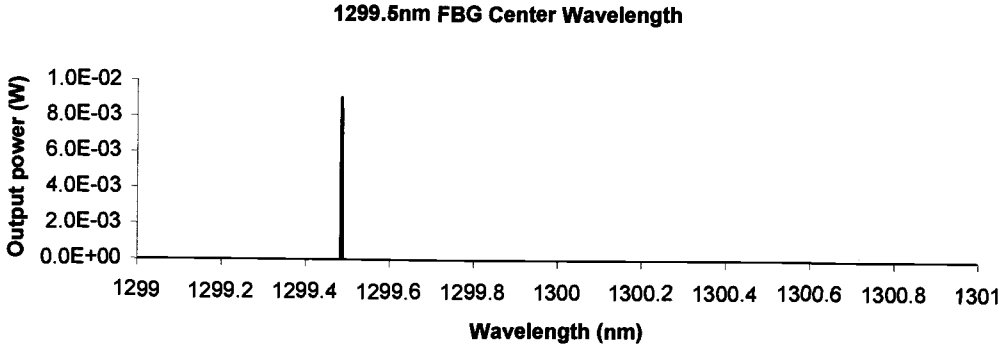

Figure 5.8 Plot of the calculated device output with a grating center wavelength of 1299.5nm and a linear amplitude scale. Side modes are virtually invisible on the linear scale.

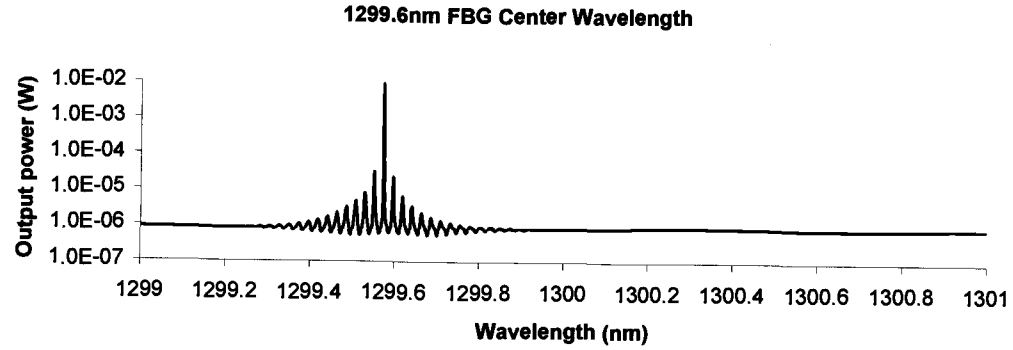

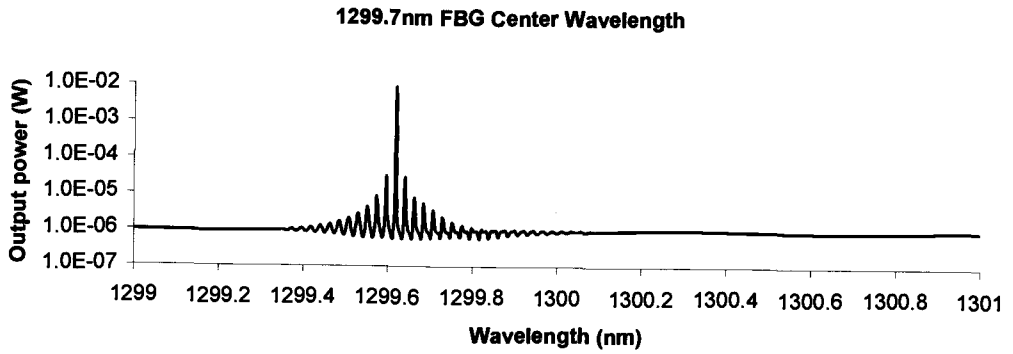

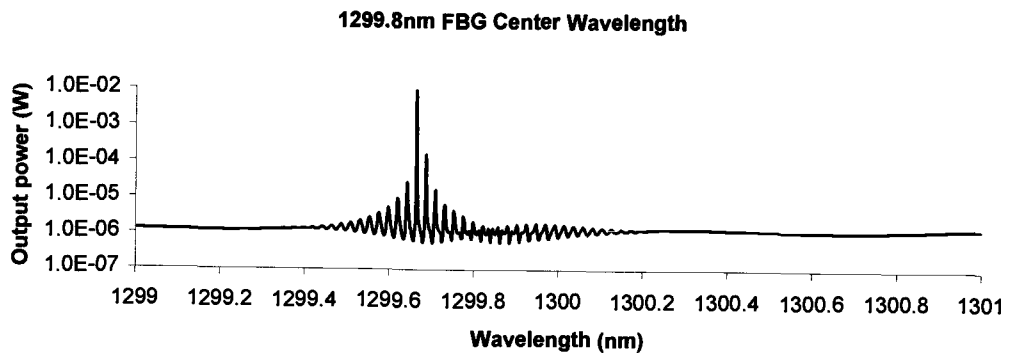

Figures 5.9a-c Three plots of the calculated device output with three different grating wavelengths and a logarithmic amplitude scale to illustrate side mode behavior. Note that the side modes gain intensity as the center wavelength of the FBG is increased and approaches a minimum in the bare laser cavity modes.

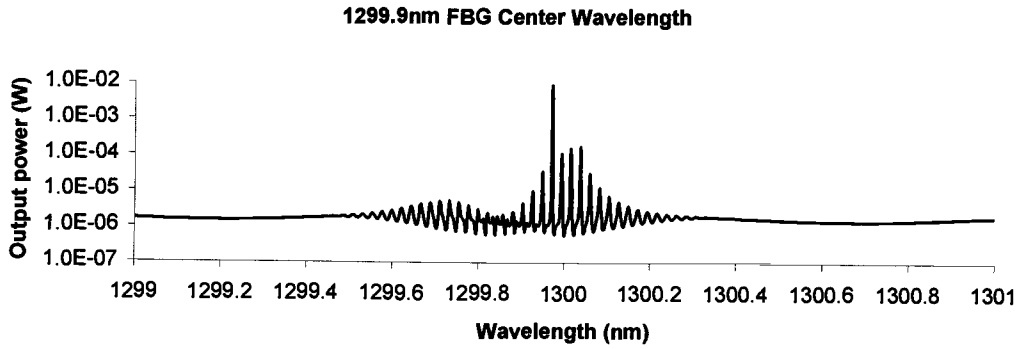

Figure 5.9d Plot of the calculated device output with a FBG center wavelength of 1299.9nm and a logarithmic scale. Note that the center wavelength has jumped substantially between this plot and plot 5.8c, above. Two regions of higher amplitude side modes are visible with a null region between that corresponds to a minimum in the bare laser diode cavity modes.

The mode-hop behavior visible between plots 5.8c and 5.8d illustrate how the residual cavity modes from the bare laser diode prevent continuous tuning of the output wavelength of the FBG coupled laser device. The mode structure of the bare laser diode, with mode spacing of approximately 0.75 nm, exhibits another minimum near 1300.6 nm. Figure 5.9 illustrates this hop in the mode structure. Note that the center wavelengths of the calculated output spectra are substantially different from the actual center wavelengths of the FBG, illustrating the mode-pulling effects of the original cavity modes on the output spectra of the laser diode.

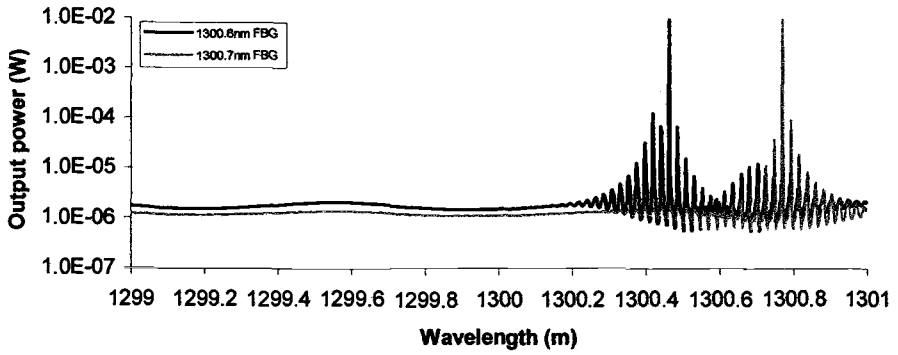

Figure 5.10 Plot illustrating mode hop behavior near 1300.6 nm.

To further illustrate the mode pulling and mode-hop behavior, the laser diode model program was run using the same parameters for injection current, AR coating, and FBG reflectivity for FBG center wavelengths from 1295 nm to 1305 nm, in increments of 0.1nm. The resulting dominant lasing wavelength was recorded for each of these 100 points and is plotted as output wavelength versus FBG center wavelength in Figure 5.10, below. Mode-hops are visible as sudden vertical displacements in the plot.

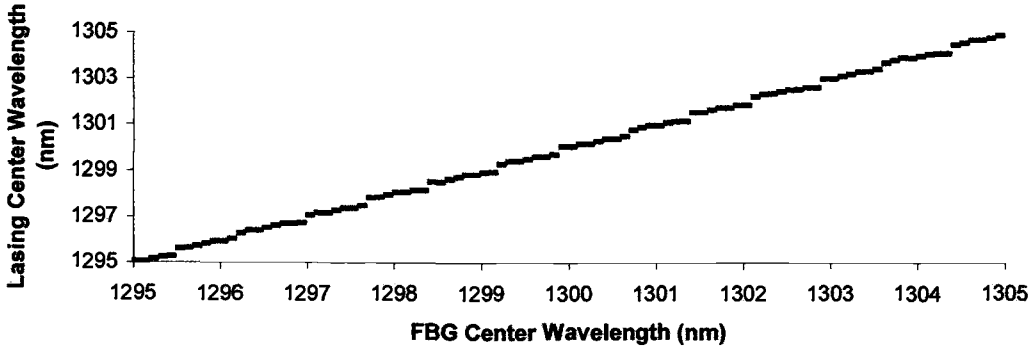

Figure 5.11 Plot of lasing wavelength versus FBG center wavelength, illustrating periodic mode-hop behavior.

Chapter Six

Conclusions

This thesis has presented a new computer solution of the coupled cavity model for an antireflection coated, FBG coupled, tunable laser diode device and has included a discussion of the fabrication and characteristics of an antireflection coated FBG coupled tunable laser diode. Both the construction and modeling of the device were described and experimental and theoretical results were compared. The coupled cavity model produces output that agrees with the output of the actual device. This chapter will review the results of the research and outline possible avenues of future research on the topic.

6.1 Summary of Results

An AR-coated laser device was fabricated through the thermal evaporation of a single layer of SiO onto a standard 1300nm Fabry-Perot laser diode. This device was coupled into an optical fiber containing an optical fiber Bragg grating which served as a narrow bandwidth front reflector for the laser system. Applying axial strain to the FBG allowed the center wavelength of the resulting laser to be tuned. Unfortunately, continuous tuning of the center wavelength was not achieved due to an imperfect AR coating.

The FBG-coupled laser device was modeled using a program written in C++ using a coupled cavity approach. To our knowledge, this is the first coupled cavity model for an FBG-tuned diode laser. Cavity lifetimes, gain profiles, antireflection coatings, and FBG reflectivites were calculated and included in the model. Calculated output spectra from the coupled cavity model exhibited similar behavior to physical laser diodes. Laser turn-on behavior, widening of the spectral structure due to an antireflection coating, and tuning of the output wavelength of the FBG-coupled laser device at different grating center wavelengths were all observed and plotted. Continuous tuning was not predicted by the model for the imperfect single layer antireflection coating and was not observed in the physical device. In addition, the coupled cavity model allowed computation and observation of behavior not measurable on an optical spectrum analyzer, such as the beating between two slightly different and closely spaced mode structures.

6.2 Further Research Possibilities

Despite substantial research progress on both the construction of the FBG coupled laser device and the coupled cavity model, several possibilities exist for future research, both on the model and the device. Due to the relative simplicity of the current coupled cavity model, several improvements in the model can be made. In addition, improvements in the device are also possible.

The coupled cavity program has been written in a way that allows easy inclusion of additional dielectric sections. The effects of multilayer antireflection

coatings on the residual laser cavity modes and on the ability to continuously tune the lasing wavelength could be modeled by including extra dielectric layers on the front facet of the laser diode in the coupled cavity model. Additionally, the effects of antireflection coatings on the optical fiber end could be similarly modeled by including dielectric layers on the fiber end. Coupling losses between the laser diode and optical fiber could also be modeled using a dielectric section with a complex index of refraction.

The modeling approach of the FBG in the coupled cavity model could include chirped grating effects by allowing the reflector position to have wavelength dependence. A properly chosen grating chirp could provide interesting effects on the side mode structure. As computational power continues to increase, the FBG could be modeled directly as a series of thousands of individual index of refraction changes rather than just as a single reflector. This could allow predictions of behavior due to both stitches in gratings due to errors in the phase mask and non-uniform index modulation due to non-uniform laser illumination.

Heating and gain saturation effects were not included in the coupled cavity model or the parabolic gain profile calculation. Gain saturation effects could be included in the gain profile calculation as well as shifts in the gain curve at different temperatures. Using the thermal expansion and thermo-optic coefficients for the laser diode material, temperature effects on the mode structure of the laser could also be included.

Laser diode turn-on amplitude and bandwidth oscillations could be modeled by outputting non-averaged spectra at given time intervals. Pulsed current effects

could then be modeled by allowing the current to vary with time. One possible case to examine would be the laser output for a laser driven by a high-current, short time duration pulse. Bob McMahon from Blue Road Research has constructed a pulse driver circuit that achieves this and sent the circuit to OSU [49]. Preliminary results indicate a broad output spectrum from the laser diode.

Further research on the laser device could include improving the antireflection coatings on the laser diode to minimize residual mode structure, improving the coupling between the laser diode and fiber, use of very narrow bandwidth gratings with varying reflectivities, and the use of novel grating structures on the output of the laser diode, such as broad, chirped gratings and gratings written in polarization-maintaining fiber with the fast axis of the fiber oriented at 45° to the direction of the polarization of the laser diode so that light is launched into both polarizations. Additionally, the FBG could be moved farther from the laser diode so that it is located outside of the coherence length of the laser.

Bibliography

1. T. Erdogan, "Fiber Grating Spectra", *Journal of Lightwave Technology*, 1997, 15, pp. 1277-1293.

2. K.O. Hill , Y. Fujii, D.C. Johnson, and B.S. Kawasaki, "Photosensitivity in Optical Fiber Waveguides: Application to Reflection Filter Fabrication", *Applied Physics Letters*, 1978, 31, pp. 647-649.

3. K.O. Hill and G. Meltz, "Fiber Bragg Grating Technology Fundamentals and Overview", *Journal of Lightwave Technology*, 1997, 15, 8, pp. 1263-1275.

4. A. Othonos and K. Kalli, *Fiber Bragg Gratings*, Artech House, (1999).

5. G. Meltz and W. W. Morey, *Conference on Optical Fiber Communication*, 1991, Paper TuM2.

6. C.R. Giles, "Lightwave Applications of Fiber Bragg Gratings", *Journal of Lightwave Technology*, 1997, 15, 8, pp. 1391-1404.

7. T. Clark and E. Udd, "Fiber Optic Grating Sensor Systems for Sensing Environmental Effects", United States Patent 5,380,995, Jan. 10, 1995.

8. E. Udd and A. Weisshaar, "High Speed Demodulation Systems for Fiber Optic Grating Sensors", United States Patent 6,335,524, Jan. 1, 2002.

9. A. Kersey and W. Morey, "Multi-element Bragg-grating Based Fibre-laser Strain Sensor", *Electronics Letters*, 1993, 29, pp. 964-966.

10. A. Kersey et al., "Fiber Grating Sensors", *IEEE Journal of Lightwave Technology*, 1997, 15, pp. 1442-1463.

11. M. Davis et al., "Interrogation of 60 Fiber Bragg Grating Sensors With Microstrain Resolution Capability", *Electronics Letters*, 1996, 32, pp. 1393-1394.

12. B. Pezeshki, "New Approaches to Laser Tuning", Optics and Photonics News, May 2001, pp.34-38.

13. L. Poyntz-Write and P. Russel, "Spontaneous Relaxation Processes in Irradiated Germanosilicate Optical Fibers", *Electronics Letters*, 1989, 25, pp. 478-479.

14. V. Bagratashivili et al., "Direct Observation of Ultraviolet Laser Induced Photocurrent in Oxygen Deficient Silica and Germanosilicate Glasses", *Applied Physics Letters*, 1996, **68**, 12, pp. 1616-1618.

15. L. Dong et al., "Photoinduced Absorption Change in Germanosilicate Preforms: Evidence for the Color Center Model of Photosensitivity", *Applied Optics*, 1995, **34**, 18, pp. 3436-3440.

16. D. Williams, et al., "Direct Observation of UV-induced Bleaching of the 240 nm Absorption Band in Photosensitive Germanosilicate Glass Fibers", *Electronics Letters*, 1992, **28**, pp. 369.

17. V. Grubsky, D. Starodubov, and J. Feonberg, "Mechanisms of Index Change Induced by Near-UV Light in Hydrogen-Loaded Fibers", Conference on Bragg Gratings, Photosensitivity, and Poling in Glass Fibers and Waveguides: Applications and Fundamentals, *Optical Society of America Technical Digest Series*, 1997, 17, pp. 98-100.

18. F. Payne, "Photrefractive Gratings in Single-Mode Optical Fibers", *Electronics Letters*, 1989, **25**, pp. 498-499.

19. D. Wong, S. Poole, and M. Sceats, "Stress-Birefringence Reduction in Elliptical-Core Fibers Under Ultraviolet Irradiation", *Optics Letters*, 1992, 17, pp. 1773-1775.

20. P. Lemaire, et al., "High-pressure H_2 Loading as a Technique for Achieving Ultrahigh UV Photosensitivity and Thermal Sensitivity in GeO_2 Doped Optical Fibres", *Electronics Letters* 1993, 29, pp. 1191-1193.

21. F. Bilodeau, et al., "Photosensitization of Optical Fiber and Silica-on-silicon/silica Waveguides", *Optics Letters*, 1993, **18**, pp. 953-955.

22. K. O. Hill, et al., "Bragg Gratings Fabricated in Monomode Photosensitive Optical Fiber by UV Exposure Through a Phase Mask", *Applied Physics Letters*, 1993, 62, pp. 1035-1037.

23. D. Andersen, et al., "Production of In-fiber Gratings Using a Diffractive Optical Element", *Electronics Letters*, 1993, 29, pp. 566-568.

24. G. Meltz, W. Morey, and W. Glenn, "Formation of Bragg Gratings in Optical Fibers by a Transverse Holographic Method", *Optics Letters* 1989, 14, pp. 823-825.

25. K. Stump, T.K. Plant, and Y. Sun, "Variable Wavelength Fiber Gratings Written with a Diffractive Optical Element", *Electronics Letters*, 2000, **36**, 6, pp. 567-569.

26. P. Dyer, R. Farley, and R. Giedl, "Analysis and Application of a 0/1 Order Talbot Interferometer for 193 nm laser grating formation", *Optics Communications*, 1996, **129**, pp. 98-108.

27. L. Vaughan, "Low-cost Optical Fiber Grating Sensor System", Master's Thesis, Oregon State University, 2001.

28. G. Agrawal and N. Dutta, *Semiconductor Lasers, 2nd Edition*, Van Nostrand Reinhold, 1993.

29. K. Kuhn, *Laser Engineering*, Prentice Hall, 1998.

30. G. Thompson *Physics of Semiconductor Laser Devices*, John Wiley & Sons, 1980.

31. P. Green, *Fiber Optics Networks*, Prentice Hall, 1993.

32. D. Ericksen, "Methods of Tuning Diode Laser Wavelengths", OSU FBG Group Meeting Presentation, 2002.

33. D. Bird et al., "Narrow Line Semiconductor Laser Using Fiber Grating", *Electronics Letters*, 1991, **27**, pp. 1115-1116.

34. R. Kashyap, "Wavelength Uncommitted Lasers", *Electronics Letters*, 1994, **30**, pp. 1095-1096.

35. I. Pierce, P. Rees, and P. Spencer, "Multimode dynamics in laser diodes with optical feedback", Physical Review A 2000, **61**, 4.

36. R. Lang and K. Kobayashi, "External Optical Feedback Effects on Semiconductor Injection Laser Properties", *IEEE Journal of Quantum Electronics*, 1980, **16**, 347.

37. J.M. Buldu et al., "Asymmetric and delayed activation of side modes in multimode semiconductor lasers with optical feedback", Journal of Optics B: Quantum and Semiclassical Optics 2002,**4**, pp. 415-420.

38. M. Matus, J. Moloney, and M. Kolesik, "Relavance of Symmetry for the Synchronization of Chaotic Optical Systems and the Related Lang-Kobayashi Model Limitations", *Physical Review E*, (2003) **67**.

39. W. Lamb, R. Lang, and M. Scully, "Why is the laser line so narrow? A theory of single-quasimode laser operation", *Physical Review A*, 1973, 7, 5, pp. 1788-1797.

40. K. J. Ebeling and L. A. Coldren, "Analysis of Multielement Semiconductor Lasers", *Journal of Applied Physics*, 1983, **54**, 6, pp. 2962-2969.

41. H. Ghafouri-Shiraz, *Fundamentals of Laser Diode Amplifiers*, John Wiley & Sons, 1996, pp. 49-50.

42. C. Goh et al., "Wavelength Tuning of Fiber Bragg Gratings Over 90 nm Using a Simple Tuning Package", *IEEE Photonics Technology Letters*, 2003, **15**, 4, pp. 557-559.

43. W. Press et al., *Numerical Recipes in C, 2nd Edition*, Cambridge University Press, 1992, pp. 397-408.

44. D. Vakhshoori, P. D. Wang, M. Azimi, K. J. Knopp, and M. Jiang, *Optical Fiber Conference 2001 Proceedings*, 2001, paper TuJ 1.

45. J. Stone, "Photorefractivity in GeO_2 Doped Silica Fibers", *Journal of Applied Physics*, Vol. 62, 1987, pp. 4371-4374.

46. D. Ericksen, T. Plant, and M. Winz, "Temperature and Fiber Bragg Grating Tunable Laser Diode", *Pacific Northwest Fiber Sensor Workshop Proceedings*, 2003.

47. C. Masoller, "Implications of How the Linewidth Enhancement Factor is Introduced on the Lang and Kobayashi Model", *IEEE Journal of Quantum Electronics*, **33**, 1997, p. 796.

48. A. Prasad et al., "Low-Frequency Fluctuations in External Cavity Semiconductor Lasers: Understanding Based on a Simple Dynamical Model", *Journal of Optics B: Quantum and Semiclassical Optics*, 3, 2001, p. 242

49. R. McMahon, personal conversation.

50. D. Ericksen, M.S. Thesis, Oregon State University.

Appendix

Appendix

Coupled Cavity Laser Model Program in C

// lasertheory.cpp : Main application, calculates output spectrum of laser diode with ext. refl. Program is currently set up to run parameters similar to those used in the thesis work. Additional parameters and options can be enabled through the commented out sections of the program.

```
#include "stdafx.h"


gsl_complex  number, omega, k0,k2,k3,i,n1kappa;
long double x,y,n1,kappa,Rext,z1,z2,zdiff,c,tstep; //Rext is the reflectivity of the
external cavity
long double
S[RES],g[RES],kreal[RES],mirrorlife[RES],Refl[RES],Sout[RES],length,width,depth;
long double* n = NULL;
long double* z = NULL;
gsl_complex* k = NULL;


int numsecs;

int main(void)

#define PI 3.141592654
#define HBAR 1.05e-034
{

        long double stepsize,Q,k1real,k1imag,ax,bx,cx,fa,fb,fc; //Q's are actually|Q|^2
        long double startlambda,endlambda,startk,endk,N,drivecurr,relrefl;
        int index,outerindex;
        FILE *spectrum, *mirrtau, *grating, *gainthresh;

        spectrum = fopen("spectrum.txt","w");
        mirrtau = fopen("mirrtau.txt","w");
        grating = fopen("grating.txt","r");
        gainthresh = fopen("gainthresh.txt","w");

        c = 299792458;
        tstep = 1e-15; //setting timestep to 1fs
//      n1=3.8; //setting the index of refraction in the cavity
```

```
        kappa=0; //initializing gain/loss in cavity to zero

        GSL_SET_COMPLEX(&i,0,1);
//      GSL_SET_COMPLEX(&n1kappa,n1,kappa); //n1kappa = n1 + i*Kappa --
this is an often used value

/*      GSL_SET_COMPLEX(&number,3,2);//this routine allows checking to
ensure gsl complex library is working
        GSL_SET_COMPLEX(&i,0,1);
        number = gsl_complex_exp(number);
        x = GSL_REAL(number);
        y = GSL_IMAG(number);
        printf("e^(3+2i) is %f + %fi\n",x,y);
*/
        cout << flush;
/*      cout << "Please enter the reflectivity of your external mirror. \n";
        cin >> Rext;
        cout << "Reflectivity of external cavity set to: "<< Rext << "\nz1 (diode
length) = ";
*/
//*******       cout <<"\nEnter the number of sections of the laser system, including
the gain region \nand the end mirror eg. gain, one airgap, and mirror = 3secs.\n
Numsecs: ";
//*******       cin >> numsecs;
        numsecs = 5;

        n = new long double[numsecs+1];
        z = new long double[numsecs+1];
        k = new gsl_complex[numsecs+1];

        n[0] = 1;
        z[0] = 0;

        n[1] = 3.8;

        n[2] = 1.9;
        n[3] = 1;
        n[4] = 1.5;

        z[1] = 3e-4;
        z[2] = 172e-009 + z[1];
        z[3] = 1e-006 + z[2];
        z[4] = .25 + z[3];
        relrefl = .3;
```

```
/****    cout << "\nEnter the length of the gain region (in meters): ";
        cin >> z[1];

        for (index = 2; index < numsecs; index++) {
                cout << "\nEnter the index of refraction of section number " << index
<<": ";
                cin >> n[index];
                cout << "\nEnter the length of section number " << index <<": ";
                cin >> z[index];
                z[index] = z[index] + z[index-1];
        }

        cout << "\nEnter the peak refl of the grating: ";
        cin >> relrefl;
****/

/*      Rext = sqrt(Rext); //setting R to it's square root, which is actually used in the
calc
        n[numsecs] = (n[numsecs-1]+Rext)/(n[numsecs-1]-Rext);//calc. index based
on reflectivity of mirror
*/

/*      cin >> z1;
        cout << "z1 set to: " << z1 << "\nz2 (mirror position) = ";
        cin >> z2;
        cout << "z2 set to: " << z2;
*/



//      zdiff = z2-z1;
//      cout << "\nzdiff is: " << zdiff;

        length = z[1]*100; //Converting diode length in meters to cm
        width = 10e-004; //(width of gain region in cm)
        depth = .1e-004; //(depth of gain region in cm)

        startlambda = 1.299e-006;
        endlambda = 1.301e-006;


        //converting wavelength span to wavevector span.
        // ***NOTE:  Remember k1 real is 2*Pi/wavelength in the
        medium=2*Pi*n/wavelength in vacuum***
```

```
        startk = 2*PI*n[1]/startlambda;  //(longer wavelength=smaller freq, going
        from high k to low)
        endk = 2*PI*n[1]/endlambda;

        stepsize = (startk-endk)/RES;

        k1real = startk;
        k1imag = 0;

        for (index = 0; index<RES; ++index){
                //for loop to read in grating reflectivities
                fscanf(grating, "%LE", &Refl[index]);
                Refl[index] = sqrt(relrefl*Refl[index]);//setting reflectivities to their
square roots, which are the values actually used
//              cout<<"Refl = " << Refl[index] <<"\n";

        }

        for (index = 0; index < RES; ++index){
                //for loop to calculate gain thresholds and mirror lifetimes

                kreal[index] = k1real;
                Rext = Refl[index];
                n[numsecs] = n[numsecs-1]*(1+Rext)/(1-Rext);//calc. index based on
reflectivity of mirror
                cout << "\n n = " << n[numsecs];

                Q = calcQ(k1real,k1imag);


        //********SOLVE FOR MINIMUM IN Q EQN. BY CHANGING IMAG.
PART OF K1***********
                ax = -10.0;
                bx = -5.0;
                cx =  10.0;
                fa=fb=fc=0.0;

                minbracket(k1real,&ax,&bx,&cx,&fa,&fb,&fc,calcQ);  //bracketing
minimum

                Q = brent(k1real, ax, bx, cx, calcQ, 1e-10, &k1imag);

                mirrorlife[index] = mirrorlifetime(k1real,k1imag);


                fprintf(gainthresh, "%E  \n", Q);
```

```
            fprintf(mirrtau, "%E \n",mirrorlife[index]);

            g[index] = S[index] = 0;

            k1real = k1real-stepsize;
            k1imag = 0;

            }


      drivecurr = .025;
      N = 0;

      printf("\n\nEntering photon density for loop");

      for(outerindex = 0; outerindex<10e-9/tstep; ++outerindex){
            //iterate loop many times to account for turn on transients (currently
10ns calculated)

            N = carrierdens(N,drivecurr);
            for (index = 0; index < RES; ++index){//loop to calc. carrier dens.,
gain, and photon dens.

                  g[index] = gaincalc(kreal[index],N);
                  S[index] = photondens(N,S[index],g[index],mirrorlife[index]);

            }

      }


      printf("\n\nEntering averaging for loop");

      for(outerindex = 0; outerindex<1 /*10e-9/tstep*/; ++outerindex){
            //iterate loop many times to average output (currently 10ns calculated)

            N = carrierdens(N,drivecurr);
            for (index = 0; index < RES; ++index){//loop to calc. carrier dens.,
gain, and photon dens.

                  g[index] = gaincalc(kreal[index],N);
                  S[index] = photondens(N,S[index],g[index],mirrorlife[index]);
                  Sout[index] = Sout[index] + S[index];

            }
```

```
	}

	for (index = 0; index < RES; ++index){//outputting data to file
		S[index] = Sout[index]/1/*(10e-9/tstep)*/;
		fprintf(spectrum, "%E	%E \n",2*PI*n[1]/kreal[index]
,HBAR*c/n[1]*kreal[index]*length*width*depth*S[index]/(1/(1/mirrorlife[index]-
1/4.7e-012)));

	}


	cout << "\nThe end is near!";
	fclose(spectrum);


	return 0;
}



// calcQ.cpp : Routine to calculate output of complex eqn. Q

#include "stdafx.h"



extern gsl_complex  number, omega, k0,k2,k3,i,n1kappa;
extern long double x,y,n1,kappa,Rext,z1,z2,zdiff; //Rext is the reflectivity of the
external cavity
extern int numsecs;
extern long double* n;
extern long double* z;
extern gsl_complex* k;

long double calcQ(long double k1real, long double k1imag)
//***This routine returns the abs. value of the complex equation Q.  See eqn 10, phys
rev. a 61 053801 ***



{
	int index;
	gsl_complex Q,q11,q12,q21,q22,temp11,temp12,temp21,temp22,k1;
	long double Qsquare;
	gsl_complex* Q11 = new gsl_complex[numsecs];
	gsl_complex* Q12 = new gsl_complex[numsecs];
```

```
gsl_complex* Q21 = new gsl_complex[numsecs];
gsl_complex* Q22 = new gsl_complex[numsecs];


// setting k's based on k1.
GSL_SET_COMPLEX(&k1,k1real,k1imag);
GSL_SET_REAL(&k[0],GSL_REAL(k1)/n[1]*n[0]);
GSL_SET_IMAG(&k[0],0);

k[1] = k1;

for (index = 2; index < numsecs; index++) {
        GSL_SET_REAL(&k[index],GSL_REAL(k1)/n[1]*n[index]);
        GSL_SET_IMAG(&k[index],0);
}

k[numsecs]=gsl_complex_mul_real(k[0],n[numsecs-1]*(1+Rext)/(1-Rext));

//calculating Q matrix elements


for(index = 0; index < numsecs; index++) {

        Q11[index] =
gsl_complex_mul(gsl_complex_div(gsl_complex_add(k[index+1],k[index]),gsl_compl
ex_mul_real(k[index+1],2)),\

    gsl_complex_exp(gsl_complex_mul(i,gsl_complex_mul_real(gsl_complex_sub
(k[index+1],k[index]),z[index]))));

        Q12[index] =
gsl_complex_mul(gsl_complex_div(gsl_complex_sub(k[index+1],k[index]),gsl_compl
ex_mul_real(k[index+1],2)),\

    gsl_complex_exp(gsl_complex_mul(i,gsl_complex_mul_real(gsl_complex_add
(k[index+1],k[index]),z[index]))));

        Q21[index] =
gsl_complex_mul(gsl_complex_div(gsl_complex_sub(k[index+1],k[index]),gsl_compl
ex_mul_real(k[index+1],2)),\

    gsl_complex_exp(gsl_complex_mul(gsl_complex_negative(i),gsl_complex_mu
l_real(gsl_complex_add(k[index+1],k[index]),z[index]))));
```

```
		Q22[index] =
gsl_complex_mul(gsl_complex_div(gsl_complex_add(k[index+1],k[index]),gsl_compl
ex_mul_real(k[index+1],2)),\

	gsl_complex_exp(gsl_complex_mul(gsl_complex_negative(i),gsl_complex_mu
l_real(gsl_complex_sub(k[index+1],k[index]),z[index]))));
	}

	//multiplying out Q matrix elements to get the Q11 element of the overall
matrix.
	q11 = Q11[0];
	q12 = Q12[0];
	q21 = Q21[0];
	q22 = Q22[0];

	for(index = 1; index < numsecs; index++) {
		temp11 =
gsl_complex_sub(gsl_complex_mul(Q11[index],q11),gsl_complex_mul(Q12[index],
q21));
		temp12 =
gsl_complex_sub(gsl_complex_mul(Q11[index],q12),gsl_complex_mul(Q12[index],
q22));
		temp21 =
gsl_complex_sub(gsl_complex_mul(Q21[index],q11),gsl_complex_mul(Q22[index],
q21));
		temp22 =
gsl_complex_sub(gsl_complex_mul(Q21[index],q12),gsl_complex_mul(Q22[index],
q22));

		q11 = temp11;
		q12 = temp12;
		q21 = temp21;
		q22 = temp22;
	}

	Q = q11;

	Qsquare = gsl_complex_abs(Q);

	return Qsquare;

} // solvers.cpp : routines to find the minimum in a complex function by varying the
complex part
//                                of the variable, while holding the real part fixed.

#include "stdafx.h"
```

```
#define SHFT(a,b,c,d) (a)=(b);(b)=(c);(c)=(d);
#define SIGN(a,b) ((b) >= 0.0 ? fabs(a) : -fabs(a))


extern gsl_complex  number, omega, k0,k2,k3,i,n1kappa;
extern long double x,y,n1,kappa,Rext,z1,z2,zdiff; //Rext is the reflectivity of the
external cavity



void minbracket(long double k1real, long double *ax, long double *bx, long double
*cx, long double *fa, long double *fb, long double *fc, long double f(long double,
long double))
//See pg. 400 of Numerical Recipes in C.  This is a routine for bracketing a minima

#define GOLD 1.618034
#define GLIMIT 100.0
#define TINY 1.0e-020


{
        long double ulim, u, r, q, dum, fu;

        *fa = f(k1real,*ax);
        *fb = f(k1real,*bx);
        if (*fb > *fa) {
                SHFT(dum, *ax, *bx, dum)
                SHFT(dum, *fb, *fa, dum)
        }
        *cx = (*bx) + GOLD*(*bx - *ax);
        *fc = f(k1real, *cx);
        while (*fb > *fc) {
                r = (*bx-*ax)*(*fb-*fc);
                q = (*bx-*cx)*(*fb-*fa);
                u = (*bx) - ((*bx-*cx)*q - (*bx-
*ax)*r)/(2.0*SIGN(GSL_MAX_LDBL(fabs(q-r),TINY),q-r));
                ulim = (*bx)+GLIMIT*(*cx-*bx);
                if((*bx-u)*(u-*cx) > 0.0) {
                        fu = f(k1real,u);
                        if (fu < *fc) {
                                *ax = *bx;
                                *bx = u;
                                *fa = (*fb);
                                *fb = fu;
                                return;
```

```
                } else if (fu > *fb) {
                        *cx = u;
                        *fc = fu;
                        return;
                }
                u = (*cx) + GOLD*(*cx-*bx);
                fu = f(k1real, u);
        } else if ((*cx - u)*(u-ulim) > 0.0) {
                fu = f(k1real,u);
                if (fu < *fc) {
                        SHFT(*bx,*cx,u,*cx+GOLD*(*cx-*bx))
                        SHFT(*fb,*fc,fu,f(k1real,u))
                }
        } else if ((u-ulim)*(ulim-*cx) >= 0.0) {
                u = ulim;
                fu = f(k1real, u);
        } else {
                u = (*cx) + GOLD*(*cx-*bx);
                fu = f(k1real, u);
        }
        SHFT(*ax,*bx,*cx,u)
        SHFT(*fa,*fb,*fc,fu)
    }
}
```

long double brent(long double k1real, long double ax, long double bx, long double cx, long double f(long double, long double), long double tol, long double *xmin)

//see pg. 404 of numerical recipes in c. this is a routine for Brent's method of finding a minima

```
#define ITMAX 100
#define CGOLD 0.3819660
#define ZEPS 1.0e-10


{
        int iter;
        long double a,b,d,etemp,fu,fv,fw,fx,p,q,r,tol1,tol2,u,v,w,x,xm;
        long double e = 0.0;

        a = (ax < cx ? ax : cx);
        b = (ax > cx ? ax : cx);
        x=w=v=bx;
        fw=fv=fx=f(k1real, x);
        for (iter=1;iter<=ITMAX;iter++) {
```

```
        xm = 0.5*(a+b);
        tol2=2.0*(tol1=tol*fabs(x)+ZEPS);
        if (fabs(x-xm) <= (tol2-0.5*(b-a))) {
                *xmin=x;
                return fx;
        }
        if (fabs(e) > tol1) {
                r=(x-w)*(fx-fv);
                q=(x-v)*(fx-fw);
                p=(x-v)*q-(x-w)*r;
                q=2.0*(q-r);
                if (q > 0.0) p = -p;
                q=fabs(q);
                etemp=e;
                e=d;
                if (fabs(p) >= fabs(.05*q*etemp) || p <= q*(a-x) || p>= q*(b-x))
                        d=CGOLD*(e=(x >= xm ? a-x : b-x));
                else {
                        d=p/q;
                        u=x+d;
                        if (u-a < tol2 || b-u < tol2)
                                d=SIGN(tol1,xm-x);
                }
        } else {
                d=CGOLD*(e=(x >= xm ? a-x : b-x));
        }
        u=(fabs(d) >= tol1 ? x+d : x+SIGN(tol1,d));
        fu=f(k1real,u);

        if(fu <= fx) {
                if (u >= x) a=x; else b=x;
                SHFT(v,w,x,u)
                SHFT(fv,fw,fx,fu)
        } else {
                if (u < x) a=u; else b=u;
                if (fu <= fw || w == x) {
                        v=w;
                        w=u;
                        fv=fw;
                        fw=fu;
                } else if (fu <= fv || v == x || v == w) {
                        v=u;
                        fv=fu;
                }
        }
}
```

```
        cout << "Too many iterations in minimum solver.";
        cout << flush;
        getch();
        *xmin=x;
        return fx;
}

// mirrorlifetime.cpp : Routine to calculate cavity lifetimes
#include "stdafx.h"


extern gsl_complex  number, omega, k0,k2,k3,i,n1kappa;
extern long double x,y,n1,c,kappa,Rext,z1,z2,zdiff; //Rext is the reflectivity of the
external cavity
extern int numsecs;
extern long double* n;
extern long double* z;
extern gsl_complex* k;


long double mirrorlifetime(long double k1real, long double k1imag)
//***This routine returns the value of the "mirror lifetime"  see eqn 19, phys rev. a 61
053801 ***

#define LIFETIME 4.7e-012  // absorption lifetime from Ebeling and Coldren paper

{
        long double tau,gthresh,z0=0;
        int index;

        gsl_complex k1;
        gsl_complex* a = new gsl_complex[numsecs];
        gsl_complex* b = new gsl_complex[numsecs+1];
        gsl_complex* Q11 = new gsl_complex[numsecs];
        gsl_complex* Q12 = new gsl_complex[numsecs];
        gsl_complex* Q21 = new gsl_complex[numsecs];
        gsl_complex* Q22 = new gsl_complex[numsecs];


        // setting k's based on k1.
        GSL_SET_COMPLEX(&k1,k1real,k1imag);
        GSL_SET_REAL(&k[0],GSL_REAL(k1)/n[1]*n[0]);
        GSL_SET_IMAG(&k[0],0);

        k[1] = k1;
```

```
        for (index = 2; index < numsecs; index++) {
                GSL_SET_REAL(&k[index],GSL_REAL(k1)/n[1]*n[index]);
                GSL_SET_IMAG(&k[index],0);
        }

        k[numsecs]=gsl_complex_mul_real(k[0],n[numsecs-1]*(1+Rext)/(1-Rext));

        gthresh = -2*k1imag;

        for(index = 0; index < numsecs; index++) {

                Q11[index] =
gsl_complex_mul(gsl_complex_div(gsl_complex_add(k[index+1],k[index]),gsl_compl
ex_mul_real(k[index+1],2)),\

        gsl_complex_exp(gsl_complex_mul(i,gsl_complex_mul_real(gsl_complex_sub
(k[index+1],k[index]),z[index])));

                Q12[index] =
gsl_complex_mul(gsl_complex_div(gsl_complex_sub(k[index+1],k[index]),gsl_compl
ex_mul_real(k[index+1],2)),\

        gsl_complex_exp(gsl_complex_mul(i,gsl_complex_mul_real(gsl_complex_add
(k[index+1],k[index]),z[index])));

                Q21[index] =
gsl_complex_mul(gsl_complex_div(gsl_complex_sub(k[index+1],k[index]),gsl_compl
ex_mul_real(k[index+1],2)),\

        gsl_complex_exp(gsl_complex_mul(gsl_complex_negative(i),gsl_complex_mu
l_real(gsl_complex_add(k[index+1],k[index]),z[index])));

                Q22[index] =
gsl_complex_mul(gsl_complex_div(gsl_complex_add(k[index+1],k[index]),gsl_compl
ex_mul_real(k[index+1],2)),\

        gsl_complex_exp(gsl_complex_mul(gsl_complex_negative(i),gsl_complex_mu
l_real(gsl_complex_sub(k[index+1],k[index]),z[index])));
        }


        a[1] = Q11[0]; //Reminder:  taking a[0] = 1 and b[0] = 0
        b[1] = Q21[0];

        for(index = 2; index < numsecs; index++) {
```

```
                a[index] = gsl_complex_add(gsl_complex_mul(Q11[index-1],a[index-
1]),gsl_complex_mul(Q12[index-1],b[index-1]));
                b[index] = gsl_complex_add(gsl_complex_mul(Q21[index-1],a[index-
1]),gsl_complex_mul(Q22[index-1],b[index-1]));
        }

        //not calculating last "a" term as it should = 0
        b[numsecs] = gsl_complex_add(gsl_complex_mul(Q21[numsecs-
1],a[numsecs-1]),gsl_complex_mul(Q22[numsecs-1],b[numsecs-1]));

        tau = 0;
        tau = n[1]*n[1]*(gsl_complex_abs2(a[1])*(1-exp(-
gthresh*z[1]))+gsl_complex_abs2(b[1])*(exp(gthresh*z1)-1));

        for(index = 2; index < numsecs; index++) {

                tau = tau +
2*(gsl_complex_abs2(a[index])+gsl_complex_abs2(b[index]))*(z[index]-z[index-1]);
        }

        tau = tau/(2*c*gthresh*(1+n[numsecs]*gsl_complex_abs2(b[numsecs])));

        // Note:  This tau does not include scattering losses.

        tau = 1/(1/tau + 1/LIFETIME);  //Including scattering

        return tau;

}

// gaincalc.cpp : Routine to calculate the gain using a parabolic gain model
#include "stdafx.h"


// extern (put external variables needed here)
extern long double n1;
extern long double* n;

long double gaincalc(long double k1real, long double N)
//*** This routine calculates the gain at a particular wavelength using a parabolic
model.
//              see Ebeling and Coldren, J. Appl. Phys. Vol. 54, No. 6, June 1983
pg.2967 eqn. 21

#define A 2e-006 //(cm^-3)
#define B 2e009  //(micron^-2*sec^-1)
```

```
#define N0 4.5e017 //(cm^-3)
#define peaklambda 1.3

{

        long double gain, lambda;

        lambda = 1e006*2*3.14159/k1real*n[1];  //calculating wavelength in microns

        gain = A*(N-N0)-B*(peaklambda-lambda)*(peaklambda-lambda);

        return gain;
}

// carrierdens.cpp : Routine to calculate the carrier density in the gain region.

#include "stdafx.h"

extern long double S[RES],g[RES],z1,c,n1,length,width,depth,tstep;
extern long double* n;

long double carrierdens(long double N, long double current)

//#define TIMESTEP 1e-014  // making timesteps = 10fs
#define LIFETIME 3e-009  // Spontaneous emission lifetime

{
        long double q,dN,sum;
        int i;


        q = 1.6022e-019;

        dN = 0;
        sum = 0;

        for (i = 0; i<RES;++i)  {
                if (S[i]*g[i]>0)
                        sum = sum + (c/n[1]/100)*S[i]*g[i];  //dividing by 100 to
convert to cm/s
        }
//      cout << "\n term = "<<S[1];
//      cout << flush;
//      _getch();
        dN = current/(length*width*depth*q) - N/LIFETIME - sum;
```

```
        N = N + dN*tstep;

        return(N);
}

// photondens.cpp : Routine to calculate photon densities
#include "stdafx.h"

extern long double c,n1,tstep;
extern long double* n;

//#define TIMESTEP 1e-014 //making timesteps = 10fs

long double photondens(long double N, long double S, long double gain, long
double mirrorlife)

#define LIFETIME 3e-009  // Spontaneous emission lifetime

{
        long double dS,semission,confinement;

        confinement = .75;
        semission = 1e-004; //(spontaneous emission coupling factor)
        dS = 0;

        dS = confinement*semission*N/LIFETIME +
(confinement*gain*c/n[1]/100)*S - S/mirrorlife;
        //dividing by 100 to convert from meters to cm/s

        S = S + dS*tstep;
        if(S<0) S=0;

        return(S);
}
```